Title
White Matter Stroke Induces a Unique Oligo-Astrocyte Niche That Inhibits Recovery

Journal
Journal of Neuroscience, 39(47)

ISSN
0270-6474

Authors
Sozmen, Elif G
DiTullio, David J
Rosenzweig, Shira
et al.

Publication Date
2019-11-20

DOI
10.1523/jneurosci.0103-19.2019

Peer reviewed

Development/Plasticity/Repair

White Matter Stroke Induces a Unique Oligo-Astrocyte Niche That Inhibits Recovery

Elif G. Sozmen,[1]* David J. DiTullio,[1]* Shira Rosenzweig,[1] Jason D. Hinman,[1] Sam P. Bridges,[1] Miguel Alejandro Marin,[1] Riki Kawaguchi,[2] Giovanni Coppola,[2] and S. Thomas Carmichael[1]

[1]Department of Neurology, David Geffen School of Medicine at UCLA Health Sciences, Los Angeles, California 90095, and [2]Department of Psychiatry, Semel Institute for Neuroscience and Human Behavior, David Geffen School of Medicine at UCLA, Los Angeles, California 90095

Subcortical white matter stroke is a common stroke subtype. White matter stroke stimulates adjacent oligodendrocyte progenitor cells (OPCs) to divide and migrate to the lesion, but stroke OPCs have only a limited differentiation into mature oligodendrocytes. To understand the molecular systems that are active in OPC responses in white matter stroke, OPCs were virally labeled and laser-captured in the region of partial damage adjacent to the infarct in male mice. RNAseq indicates two distinct OPC transcriptomes associated with the proliferative and limited-regeneration phases of OPCs after stroke. Molecular pathways related to nuclear receptor activation, ECM turnover, and lipid biosynthesis are activated during proliferative OPC phases after stroke; inflammatory and growth factor signaling is activated in the later stage of limited OPC differentiation. Within ECM proteins, Matrilin-2 is induced early after stroke and then rapidly downregulated. Prediction of upstream regulators of the OPC stroke transcriptome identifies several candidate molecules, including Inhibin A-a negative regulator of Matrilin-2. Inhibin A is induced in reactive astrocytes after stroke, including in humans. In functional assays, Matrilin-2 induces OPC differentiation, and Inhibin A inhibits OPC Matrilin-2 expression and inhibits OPC differentiation. *In vivo*, Matrilin-2 promotes motor recovery after white matter stroke, and promotes OPC differentiation and ultrastructural evidence of remyelination. These studies show that white matter stroke induces an initial proliferative and reparative response in OPCs, but this is blocked by a local cellular niche where reactive astrocytes secrete Inhibin A, downregulating Matrilin-2 and blocking myelin repair and recovery.

Key words: **NG2; oligodendrocyte; precursor; remyelination; repair**

Significance Statement

Stroke in the cerebral white matter of the brain is common. The biology of damage and recovery in this stroke subtype are not well defined. These studies use cell-specific RNA sequencing and gain-of-function studies to show that white matter stroke induces a glial signaling niche, present in both humans and mice, between reactive astrocytes and oligodendrocyte progenitor cells. Astrocyte secretion of Inhibin A and downregulation of oligodendrocyte precursor production of Matrilin-2 limit OPC differentiation, tissue repair, and recovery in this disease.

Introduction

White matter stroke constitutes up to 25% of all stroke subtypes and accumulates to produce the second most common form of dementia, vascular dementia (Iadecola, 2013). Unlike large artery stroke, white matter stroke occurs in the subcortical white matter, with greatest frequency near the lateral ventricles (DeCarli et al., 2005). There is no therapy that promotes tissue repair or recovery in white matter stroke. We have recently characterized white matter stroke in a mouse model that closely parallels the human disease. White matter stroke produces a central area of total cellular loss, and an adjacent area of limited oligodendrocyte (OL), myelin, and axonal damage (Sozmen et al., 2009, 2016; Rosenzweig and Carmichael, 2013) that is very similar to that seen in humans (Hinman et al., 2015). Axonal damage is progressive in

Received Jan. 13, 2019; revised Aug. 21, 2019; accepted Sept. 8, 2019.

Author contributions: E.G.S., D.J.D., S.R., J.D.H., S.P.B., M.A.M., R.K., G.C., and S.T.C. designed research; E.G.S., D.J.D., S.R., J.D.H., S.P.B., M.A.M., R.K., G.C., and S.T.C. performed research; E.G.S., D.J.D., S.R., J.D.H., S.P.B., M.A.M., R.K., G.C., and S.T.C. analyzed data; E.G.S. and S.T.C. wrote the first draft of the paper; E.G.S., D.J.D., S.R., J.D.H., S.P.B., M.A.M., R.K., G.C., and S.T.C. edited the paper; E.G.S. and S.T.C. wrote the paper.

This work was supported by National Institutes of Health/National Institute of Neurological Disorders and Stroke NS102185, NS071481, and AHA14BFSC17760005, and the Dr. Miriam and Sheldon G. Adelson Medical Research Foundation. We thank the UCLA Neuropathology Core for assistance in analysis of human postmortem specimens; and Natalie Shih and Kim Vu for virus and immunohistochemistry validation studies.

The authors declare no competing financial interests.

*E.G.S. and D.J.T. contributed equally to this work.

Correspondence should be addressed to S. Thomas Carmichael at scarmichael@mednet.ucla.edu.

https://doi.org/10.1523/JNEUROSCI.0103-19.2019

this region of limited tissue damage adjacent to the stroke in both humans and mice (Gouw et al., 2008; Sozmen et al., 2009; Rosenzweig and Carmichael, 2013), establishing this area as an important target for a neural repair therapy: to prevent the slow expansion of the lesion.

In the initial response to white matter stroke, OL progenitor cells (OPCs) accumulate at the border of the infarct and proliferate. However, there is a very limited differentiation of OPCs into mature OLs, in which <10% of OPCs express markers of more mature OLs (Sozmen et al., 2016). This limited differentiation of OPCs in white matter stroke stands in contrast to other white matter diseases in the adult, such as multiple sclerosis, where OPCs differentiate and partially remyelinate the inflammatory lesion (Gallo and Armstrong, 2008; Huang et al., 2011b). To determine molecular systems that might limit OPC differentiation after stroke, we first explored known OPC signaling systems, and determined that Nogo receptor signaling through Nogo 66 receptor-1 (NgR1) limits OPC differentiation in white matter stroke (Sozmen et al., 2016). To more systematically characterize the basic biology of OPC responses in white matter stroke, allowing identification of novel targets for white matter repair, we performed RNAseq on OPCs specifically isolated from the region of partial damage adjacent to the stroke site, at an early proliferative stage (5 d after stroke) and at the later stage of limited differentiation (15 d after stroke), compared with control non-stroke OPCs. This analysis compares normal white matter OPCs with two types of poststroke OPCs: early, proliferating OPCs and later, limited differentiating OPCs. Bioinformatic analysis of this dataset indicates that stroke induces a unique transcriptional profile in OPCs, and that this profile changes over the proliferative and limited regenerative stages after stroke. One of the most differentially regulated genes in stroke OPCs over time is Matrilin-2, an extracellular matrix (ECM) adapter protein that has been linked to peripheral nerve regeneration. Predictive analysis of molecules that might regulate the stroke OPC transcriptome identified Inhibin A as a potential upstream regulator. Tissue and behavioral studies indicate that stroke induces Inhibin A expression in astrocytes in both mouse and human white matter stroke, and that this downregulates OPC Matrilin-2, limiting repair and recovery in white matter stroke.

Materials and Methods

Mice. All experiments were performed in accordance with National Institutes of Health animal protection guidelines and were approved by the University of California, Los Angeles Animal Research Committee. WT C57BL/6 (2–3 months, male) used for OPC transcriptome and OPC culture studies were obtained from The Jackson Laboratory. Aged C57BL/6 mice (18–24 months, male) were obtained from the NIA Aged Rodent Colony. Male rat pups (P6-P8) were obtained from Charles River Laboratories.

White matter stroke. White matter stroke was produced as previously described (Hinman et al., 2013; Rosenzweig and Carmichael, 2013). The vasoconstrictor N5-(1-iminoethyl)-L-ornithine (27 mg/ml in sterile physiological saline; EMD Millipore) was injected via micropipette through the cortex at an angle of 36° with a dorsomedial to ventrolateral injection path, into the white matter underlying the forelimb motor cortex. Three 200 nl injections were made in the following stereotaxic coordinates (in mm): AP: 0.22, 0.74, 1.24; ML: 0.20, 0.17, 1.15; DV: −2.20, −2.25, −2.30. Control animals underwent craniotomy alone. Aged mice received three injections of N5-(1-iminoethyl)-L-ornithine at adjusted coordinates to account for smaller brain volume. Coordinates used were as follows: AP: −0.75, −1.00, −1.25; ML: −0.96 (for all three injections); DV: −2.00, −1.95, −1.90; at an angle of 45° with a dorsoposterior to ventroanterior injection path to avoid direct damage to the forelimb motor cortex. For the comparisons, unoperated controls were used, rather than sham-injected animals. This is because of concern that needle placement and sham (such as saline injection) introduces white matter trauma and possibly vascular interruption and is not a strict sham control.

Lentivirus constructs. Expression constructs were packaged into lentiviruses and concentrated with ultracentrifugation on a sucrose button. The PDGFRα-lckGFP construct was generated with a PDGFRα promoter from a published lentiviral construct (Geller et al., 2008) to drive the expression of membrane targeted lckGFP (kind gift from Dr. Steven Green, University of Iowa). Morphologic studies of OPCs were conducted using EF1-mCherry (Systems Biosystems, CD527A-1) and MBP-GFP constructs. All lentiviruses were delivered in pulled glass micropipettes into lesioned or uninjured white matter, using timelines and stereotaxic coordinates outlined below according to their respective study protocols.

Immunohistochemistry. Immunohistochemistry was performed as described previously (Sozmen et al., 2009; Rosenzweig and Carmichael, 2013). Animals were perfused transcardially with 0.1 M PBS followed by 4% PFA. Brains were cryoprotected in 30% sucrose brains, frozen, and sectioned using a cryostat (Leica Microsystems, CM 0530) into 20–40 μm sections. Sections were blocked in 5% donkey serum, incubated with a primary antibody overnight at 4°C, incubated with a secondary antibody for 1–2 h at room temperature, and coverslipped with DPX. Slides were imaged using confocal microscopy (Nikon, C2), with imaging parameters kept constant across treatment groups within each study. For immunostaining with antibodies raised in the mouse, the mouse-on-mouse blocking kit was used to reduce nonspecific binding (Vector Labs). Primary antibodies were as follows (in alphabetical order): rabbit anti-6xHis antibody (Abcam, 1:1000), rabbit anti-Activin Receptor type IIA (ActRIIA, Abcam, 1:200), rabbit anti-Aldh1 (1:1000, Abcam), mouse anti-βIV-spectrin (1:200, Neuromab), rabbit anti-Caspr (1:500, Abcam), mouse anti-CC1 (1:200, Abcam), rabbit anti CC1 (1:100, EMD Millipore), chicken anti-GFP (1:1000, Abcam), goat anti-GFP (1:5000, gift from Dr. Nathaniel Heintz, Rockefeller University), mouse anti-glutamine synthetase (Millipore, 1:500), rabbit and goat anti-GSTπ (both 1:500, Abcam), rabbit anti-Iba1 (1:1000, Wako Chemicals), mouse anti-human Inhibinα (1:100, Abcam), rabbit anti-mouse Inhibinα (1:500, Abcam), rabbit anti-Matrilin-2 (1:200, Abcam; and 1:100, Santa Cruz Biotechnology), chicken anti-mCherry (Novus Biologicals, 1:500), rat anti-myelin basic protein (MBP, 1:1000, EMD Millipore), rabbit anti-NG2 (1:200, EMD Millipore), mouse anti-Olig1 (EMD Millipore), rat anti-Olig1 (gift from Dr. Bennett Novitch, UCLA), and rabbit anti-Olig2 (1:500, EMD Millipore). All secondary antibodies were donkey F(ab)2 fragments conjugated to cy2, cy3, or cy5 (Jackson ImmunoResearch Laboratories) and were used at a dilution of 1:500.

For quantification of immunohistochemistry, the percent of cells double-labeled with anti-Olig2 (mouse, 1:500, EMD Millipore), a transcription factor found throughout a range of the OL lineage, and with one of the following: antisera/antibodies against matrilin-2 (goat, 1:50, R&D Systems), inhibinα (rabbit, 1:100, Abcam), activin receptor 2a, and IGSF-1. The 30 μm coronal sections were stained with minimal permeabilization and treatment with Mouse on Mouse Blocker (Vector Labs). At least two sections per animal, one anterior and one posterior, with stroke involvement or equivalent sections for sham conditions were visualized. Images were acquired with a 40× oil-immersion objection (Nikon C2 confocal). All imaging parameters were kept consistent for each condition and animal. A 200 μm × 200 μm FOV was selected medial to the stroke core, localized to the white matter. Colocalized signal was defined as signal occurring in the same cell type greater than background signal. Analysis was performed by an investigator blind to treatment group.

Laser capture microdissection (LCM). Mice ($n = 10$ per group) received white matter stroke and survived to 5 and 15 d. Specific OPC labeling after stroke induction was achieved by injection of PDGFRα-lckGFP lentivirus 4 d before the designated kill time point at two sites with the following coordinates, 600 nl per site: AP: 0.50, 1.05; ML: 1.95; 1.75; DV: −1.30, −1.35. All injections were delivered at 90° angle, perpendicular to the plane of the skull. Control group brains received PDGFRα-lckGFP lentivirus in the absence of stroke and were isolated 4 d after the lentivirus delivery. Brains were isolated, snap frozen, and stored in −80°C until the

day of LCM. On the day of LCM, cryosections (20 μm) were collected on PET-membrane slides (Leica Microsystems), fixed in 90% ethanol (v/v) for 2 min, and kept in 100% ethanol. Peri-infarct white matter OPCs were detected and isolated under 40× magnification by positive GFP signal (Leica Microsystems, LMD 7000). Laser-captured cells were collected in lysis buffer (NucleoSpin RNA Isolation kit, Clontech) and DNase-treated (Clontech). RNA integrity was determined using a Bioanalyzer Picochip (Agilent Technologies) from parallel collections of a large tissue area from the sections that were used for LCM, to provide RNA concentrations within the detection range.

RNA processing and quality control. Total RNA was amplified and converted into double-stranded DNA, which is typically between 200 and 300 bp (Ovation RNAseq System version 2, Nugen) that was further processed with the Ovation UltraLow kit (Nugen). After library preparation (Encore NGS Library System I, Nugen), amplified double-stranded cDNA was fragmented into 300 bp (Covaris-S2). DNA fragments (200 ng) were end-repaired to generate blunt ends with 59 phosphatase and 39 hydroxyls and adapters ligated. The purified cDNA library products were evaluated using the Bioanalyzer (Agilent Technologies) and diluted to 10 nM for cluster generation *in situ* on the HiSeq paired-end flow cell using the CBot automated cluster generation system. All samples were multiplexed into single pools, three at a time, and run in 9 lanes total of Paired-End 2 × 100 bp flow cells in HiSeq 2000 (Illumina).

After demultiplexing samples, we obtained between 50 and 79 million reads per sample. Quality control was performed on base qualities and nucleotide composition of sequences. Alignment to the M. musculus (mm9) refSeq (refFlat) reference gene annotation was performed using the STAR spliced read aligner (Dobin et al., 2013) (PMID:23104886) with default parameters. Additional quality control was performed after the alignment to examine: the level of mismatch rate, mapping rate to the whole genome, repeats, chromosomes, and key transcriptomic regions (exons, introns, UTRs, genes). Five samples failed quality control and were excluded from further analyses. Between 65% and 81% of the reads mapped uniquely to the mouse genome. Total counts of read fragments aligned to candidate gene regions were derived using HTSeq program (http://htseq.readthedocs.io/en/release_0.9.1/) and used as a basis for the quantification of gene expression. Only uniquely mapped reads were used for subsequent analyses. Across the samples, ~25% of the annotated genes have been detected by at least 50 reads. Following alignment and read quantification, we performed quality control using a variety of indices, including sample clustering, consistency of replicates, and average gene coverage.

Bioinformatics. Differential expression analysis was performed using the EdgeR Bioconductor package (Robinson et al., 2010), and differentially expressed genes were selected based on false discovery rate (FDR) < 0.1 (Benjamini–Hochberg-adjusted p values). Day 5 ($n = 8$) and day 15 ($n = 7$) samples are compared with control samples ($n = 10$) for differential expression. Additionally, day 5 samples are compared with day 15 samples. Clustering and overlap analyses were performed using Bioconductor packages within the statistical environment R (www.r-project.org/).

Genes that were differentially expressed over two postlesion time points, and the control with FDR < 0.1 was submitted to Cluster 3.0 for hierarchical clustering analysis (Euclidian distance, centroid linkage clustering). Differentially expressed genes in the OPC transcriptomes after white matter stroke were further analyzed to identify molecular pathways, canonical signaling pathways, and upstream regulating molecules. To this end, Gene Ontology enrichment analysis was using DAVID (https://david.ncifcrf.gov/), and pathway analysis was performed using the Ingenuity Pathways Analysis software (QIAGEN, Bioinformatics). Briefly, genes differentially expressed in each comparison group in the OPC stroke transcriptome with FDR < 0.1 were compared with all genes known to be involved in a given molecular pathway, canonical signaling system, or regulated by an upstream regulator gene in a large, curated database of molecular interactions. Fisher's exact p value was calculated by IPA to identify relationship of each dataset in the OPC transcriptome to regulators, pathways, or signaling systems that were statistically significant compared with random expression patterns. Significance of upstream regulators considers four factors: (1) genes known to be regulated by the candidate upstream regulator and are differentially expressed in the OPC stroke transcriptome; (2) genes known to be regulated by the regulator but not in the OPC stroke transcriptome; (3) genes not regulated by the regulator but are in the OPC transcriptome; and (4) all genes that are themselves not regulated in the OPC transcriptome, and which are predicted to be regulated by upstream regulators in the Ingenuity Knowledge Base but not predicted to act in the OPC transcriptome. Upstream regulators were further identified based on their activation score: a score metric that predicts the strength of the induction or inhibition of a set of downstream genes from a particular upstream molecule (IPA).

Cell type enrichment analysis was performed by comparing the stroke OPC gene lists with published OPC and OL transcriptomes from rat (Nielsen et al., 2006), mouse (Cahoy et al., 2008; Zhang et al., 2014), and human (Auvergne et al., 2013). Enrichment analysis was performed by using the hypergeometric test as implemented in the R hyper function.

Confirmatory qPCR was run with cDNA on 25 genes in duplicate for each sample (Fluidigm, Biomark, 48.48 cell). ΔΔCt values were calculated compared with GAPDH and fold change calculated (Li et al., 2010; Overman et al., 2012).

Primary mouse OPC cultures. Cerebral hemispheres from 1-d-old mice were mechanically dissociated and were plated on poly-D-lysine (PDL)-coated flasks in DMEM and Ham's F12 (1:1, v/v) (Invitrogen), containing 100 μg/ml gentamycin and supplemented with 4 mg/ml dextrose anhydrous, 3.75 mg/ml HEPES buffer, 2.4 mg/ml sodium bicarbonate, and 10% (v/v) FBS (Omega Scientific). After 24 h, the medium was changed, and the cells were grown in DMEM/Ham's F12 supplemented with 5 μg/ml insulin, 50 μg/ml human transferrin, 30 nM sodium selenite, 10 mM D-biotin, 0.1% BSA (Sigma-Aldrich), 1% (v/v) horse serum, and 1% (v/v) FBS. After 9 d, OPCs were purified from the mixed glial culture by the differential shaking and adhesion procedure (Suzumura et al., 1984) and were allowed to grow on PDL-coated coverslips in a defined proliferation medium (Agresti et al., 1996), which contains 10 ng/ml PDGF-AA and 10 ng/ml bFGF (Sigma-Aldrich). OPCs were kept in proliferation medium for 4 d, passaged, and plated for testing. In studies where OPC differentiation was induced, cells were allowed to proliferate after plating for 2 d and then induced to exit from the cell cycle and differentiate by switching the cells to a mitogen-free coculture media (Oh et al., 2003). Coculture media is DMEM/Ham's F12 supplemented with 4.5 g/L D-glucose, 5 μg/ml insulin, 50 μg/ml human transferrin, 30 nM sodium selenite, 15 nM T_3 (tri-iodothyronine), 10 mM D-biotin, 10 nM hydrocortisone, 0.1% BSA, 1% (v/v) horse serum, and 1% (v/v) FBS.

Primary rat OPC cultures. Rat primary OPC cultures used for additional inhibin studies were generated using the immunopanning protocol (Dugas et al., 2010). In short, one P6-P8 brain was dissociated and passed as a single-cell suspension through three sequential panning steps, in which dishes are coated with antibodies against cell type-specific surface antigens: Ran-2 to remove astrocytes, O1 to remove OLs, and finally O4 to pull down OPCs with >99% specificity as judged by Olig2 staining. Cells were plated on PDL-coated 12-well plates at 15,000 cells/cm^2, in DMEM-Sato serum-free proliferation media supplemented with 4.2 μg/ml forskolin, 10 ng/ml CNTF, 10 ng/ml PDGF-AA, and 1 ng/ml NT-3 as outlined previously (Dugas et al., 2010).

In vitro *OPC differentiation assays.* OPCs were plated on PDL (10 μg/ml, EMD Millipore) or PDL + Matrilin-2 coated coverslips. Coverslips were coated with Matrilin-2 in the same way as PDL, by incubation in carrier free recombinant mouse Matrilin-2 (20 μg/ml, BD Biosciences). For Matrilin-2 media, Inhibin A, and Matrilin-2 + Inhibin A tests, media was supplemented with 10 μg/ml Matrilin-2 and/or 10 μg/ml carrier free mouse recombinant Inhibin A (10 μg/ml, Randox Research). Each group consisted 5 individual culture plate wells as biological replicates.

For qPCR studies, OPCs were plated in proliferation medium for 1 d, which was then exchanged for proliferation medium supplemented Matrilin-2 and/or Inhibin A as indicated. Cells were maintained for 4 d of treatment, with one-half media change every 2 d. After 4 d of incubation with test compounds, mRNA was purified from each well using the RNeasy Plus Micro Kit (QIAGEN). cDNA was reverse transcribed from

mRNA using SuperScript III Reverse Transcriptase and Oligo(dT)12–18 primer (Thermo Fisher Scientific) according to the manufacturer's protocol. qPCR was run in technical triplicate for each biological sample using the LightCycler 480 system with SYBR Green I mix (Roche Diagnostics). PCR was run with the manufacturer's default 384-well protocol, 10 μl reaction volume, and an annealing temperature of 60°C. As with qPCR tests outlined above, fold change was calculated from $\Delta\Delta$Ct values compared with *Gapdh* (Li et al., 2010; Overman et al., 2012). Paired Student's *t* test was used to compare gene expression for 5 and 15 d after stroke each to the control, nonstroke condition (for statistics, see Statistical analysis).

For MBP/Olig2 studies, cells were allowed to differentiate for 5 d in culture media and were fixed with 4% PFA, washed, and stained using a standard immunocytochemistry protocol. Olig2$^+$ cells and MBP$^+$/Olig2$^+$ double-positive cells were quantified in five separate fields using 20× magnification. The OPC differentiation index was calculated as the percentage of double-labeled cells over the total number of Olig2$^+$ cells. Photomicrographs of individual MBP-positive cells were taken at 100× magnification (7–10 per experimental group) to be used in Sholl ring analysis as described previously (Langhammer et al., 2010). Cells were skeletonized using the Glia probe of Neurolucida software (MBF Bioscience), and concentric Sholl rings were placed on each cell outline at 20 μm intervals, from which process crossings were quantified. Average number of process crossings versus diameter was graphed for each treatment group, and total number of branch points was calculated.

Human white matter stroke. To establish the relevance of Inhibin A upregulation to human white matter stroke, we examined human postmortem brain tissue specimens. The cases selected for examination in this study are autopsy cases from a clinicopathologic study of cognitively normal subjects, those with subcortical ischemic vascular dementia or Alzheimer's disease. Written informed consent for autopsy was obtained from all subjects or legal next of kin. From this larger database, cases selected for detailed microscopy. To determine the cellular localization of peri-infarct Inhibin A, we used brain sections from 2 subjects with hereditary endotheliopathy with retinopathy, nephropathy, and stroke (HEARNS) (Jen et al., 1997), which features chronic cerebral microvascular ischemia and recurrent white matter stroke and in which peri-infarct axonal changes been described (Hinman et al., 2015). Autopsies were performed ~24 h after expiration. Postmortem brain blocks were fixed for 2 weeks in formalin and paraffin embedded. Six micron sections were generated from the paraffin embedded blocks for histologic analysis using standard immunofluorescent labeling (Hinman et al., 2015; Coban et al., 2017) using primary antibodies against human GFAP (clone 2.2B10Thermo Fisher Scientific, #13-030-0; rat anti-bovine GFAP, clone 2.2B10; 1:500) and mouse anti-human Inhibin A (α chain, Abcam, 1:100), with secondary antibodies as described above.

Aged animal studies of Matrilin-2. Mice aged 21 months were obtained from NIA for a block of studies on the effect of Matrilin-2 in aged animals after white matter stroke. Mice were first trained on behavioral tasks outlined below to establish baseline performance levels. Then, at 22 months of age, white matter stroke was induced as described above. Matrilin-2 was injected 6 d after stroke as follows: a total of 1 μg of 6-His-tagged recombinant mouse matrilin-2 (2 μg/μl in PBS, R&D Systems) or 0.5 μl of PBS was injected into the stroke area via micropipette 6 d after the stroke in two 250 μl injections with coordinates AP: −0.85, −1.15; ML: −0.96 (for all three injections), DV: −1.97, −1.93. Behavioral tests were run up to 8 weeks after Matrilin-2 injection, at which time animals were killed for tissue studies. A separate cohort of animals aged 18–22 months was used for electron microscopy.

Motor function tests. Gait and forelimb function were assessed in the grid-walking task and the pasta matrix task as described previously (Rosenzweig and Carmichael, 2013). In the pasta matrix task, 21-month-old food-deprived mice were trained daily before stroke to reach through an aperture and retrieve small pieces (3.3 cm height and 1 mm diameter) of vertically oriented pasta arranged in a matrix. The number of pasta breaks per 10 min daily session was averaged across 2 consecutive days of training. Acquisition of the task was defined as a >4 average with a SD <6 of breaks. Mice that failed to learn the task after 5 weeks of training were excluded from the study. Following the stroke (or sham procedure), the mice were tested twice weekly for 8 weeks, and their performance was compared with prestroke performance. In the grid-walking task, mice were placed in a chamber with a floor made of 12 mm^2 wire mesh, with an area of 32 cm × 20 cm. A mirror was placed under the mesh, and animals were recorded as they freely walked for 5 min. Footage was analyzed by blinded raters to assess the total number of steps taken as well as the total number of foot faults. A foot fault was counted if the step placement did not provide support leading to the foot moving through the grid hole, or if the grid was at or behind the wrist. From this, a correct step percentage was calculated. Mice were tested in the grid-walking task once before the stroke to establish baseline performance levels, and then retested 1 week, 1 month, and 2 months following the stroke.

OL maturation analysis. Upon completion of the behavior study, animals were killed and tissue was prepared for immunohistochemistry as described previously. Tissue was stained with Olig2 and GSTπ, and slices were imaged using confocal microscopy. 3D distribution of OLs in the subcortical white matter was mapped using Imaris imaging software (Bitplane). OLs were initially categorized by low/high Olig2 expression and present/absent GSTπ expression into separate spot objects. The number of spots and their distance from the stroke lesion were recorded. In a subsequent analysis of OLs in these categories, expression of the Olig2 and GSTπ markers in OLs labeled with MBP-GFP lentivirus was recorded. Further morphological analysis of the subgroups was performed with Imaris filament tracing in cells labeled with EF1-mCherry lentivirus. Lentivirus injection sites were as follows: AP: −0.75, −1.00, −1.25; ML: −0.80, −1.30, −0.80; DV: −2.30, −2.30, −2.25, with 400 nl injected per site.

Matrilin-2 turnover analysis. To determine how long injected matrilin-2 remains in white matter tissue, a cohort of mice (n = 4 per group) were killed 2 h and 2, 4, and 7 d after matrilin-2 or vehicle injections into the white matter. The presence of His-tagged injected matrilin-2 was detected using immunohistochemistry. To prepare fresh tissue samples for ELISA, brains were immersed in cold PBS for 5 min, and a ~1 mm^3 segment of white matter containing the injection area was manually dissected out. The tissue was homogenized in RIPA lysis buffer (Thermo Fisher Scientific) and the supernatant incubated for 2 h in Pierce Nickel Coated Plates (Thermo Fisher Scientific) to bind the His-tagged recombinant matrilin-2 protein to the plate. Bound matrilin-2 protein was detected with HisProbe-HRP and TMB ELISA Substrate (Thermo Fisher Scientific) and the color reaction read using Alpha Innotech FluorChem FC2 Imaging System.

Electron microscopy. A separate cohort of aged animals was used for electron microscopy, following the same stroke and matrilin-2 injection protocol as outlined above (n = 5 per group). Tissue was perfused using 2% PFA/2.5% glutaraldehyde in 0.1 M phosphate buffer, dissected and immersed in the same fixative, then cut sagittally on a brain block in 1 mm sections, and a rectangle ~1 mm × 2 mm was cut from the brain slice surrounding the stroke area. This was sent to the University of Colorado Denver Anschutz Electron Microscopy Center for further processing. Briefly, the tissue was rinsed in 100 mM cacodylate buffer and then immersed in 1% osmium tetroxide and 1.5% potassium ferrocyanide for 15 min. Next, the tissue was rinsed five times in cacodylate buffer, immersed in 1% osmium for 1 h, and then rinsed again five times for 2 min each in cacodylate buffer and two times briefly in water. The tissue was transferred to graded acetone (50%, 70%, 90%, and 100%) containing 2% uranyl acetate for 15 min each. Finally, the tissue was transferred through acetone/resin mixtures at room temperature and then embedded in EMbed-812 and cured for 48 h at 60°C in an oven.

Imaging regions were determined using semithick sections (1 micron) stained with toluidine blue. Ultrathin sections (65 nm) were then cut on a Reichert Ultracut S from a small trapezoid positioned over the area of interest and were picked up on Formvar-coated slot grids (EMS). Sections were imaged on a Technai G2 transmission electron microscope (FEI) with a digital camera (AMT), and 100 μm^2 images were obtained at 11,000×. Two fields per animal were analyzed using National Institutes of Health ImageJ software. To calculate g ratios, inner and outer borders of myelin were drawn for each axon totally captured within the image field, and the ratio of inner (axon) to outer (myelin) border was calculated. Separately, total numbers of myelinated and unmyelinated axons

were counted per field. Metrics were averaged within each animal, and these animal averages were used for statistical analyses.

Experimental design and statistical analysis. All studies were analyzed with investigators blinded to treatment condition and mice randomly allocated to treatment groups. Studies were powered with sample sizes chosen to detect a statistically significant result in ANOVA with $\alpha = 0.05$ and power > 0.8 based on means and SDs in related work (Sozmen et al., 2009, 2016; Hinman et al., 2013; Rosenzweig and Carmichael, 2013). Data were tested with multiple-comparisons ANOVA and Bonferroni or Tukey-Kramer *post hoc* testing or *t* tests (GraphPad Prism 6; and Excel and Sigma-AldrichStat for behavioral tests), noted specifically for each experiment. Data from cell culture and tissue quantification studies are expressed as mean ± SEM, unless otherwise noted. Data for qPCR were tested in 5 d poststroke versus control and 15 d poststroke versus control using Student's *t* test, paired (Excel). For the RNAseq studies, 10 control, 8 d 5, and 7 d 15 poststroke samples were used, after the quality control testing. Each sample corresponds to a different mouse; 300–400 cells in 8 sections per animal were captured for RNA analysis. Bioinformatic analyses of these RNAseq studies followed the analyses described above using differential gene expression analysis, canonical pathway and molecular pathway analyses, and determination of candidate upstream regulators (Fisher's exact test and *z* score). For qRT-PCR studies, confirmatory for the RNAseq, sample size is 8 (control), 7 (5 d), and 10 (15 d) with exact *p* values reported in two-tailed *t* test comparisons between 5 or 15 d versus control. For immunohistochemical localization of Inhibin A and Matrilin-2, ActRIIA, Inhibin binding protein/p120, sample size is 6. For human brain immunohistochemical staining in control, Alzheimer's disease, and white matter stroke (HEARNS), this is a convenience sample from available autopsy material at UCLA with a sample size of 2 in HEARNS and 3 control and Alzheimer's disease cases. For the *in vitro* OPC cultures, 4–7 biological replicates with 3 technical replicates each are used. Statistics are a one-way ANOVA with Bonferroni *post hoc* testing and control for multiple comparisons. The individual *p* values, for Figure 7*a* are as follows: PDGFRa overall $p = 0.0002$, individual *p* values 0.0006, >0.9999, 0.0092, 0.9366, NG2 overall $p = 0.025$, individual *p* values 0.0118, >0.9999, 0.0043, >0.9999, MOBP overall $p = 0.0141$, individual *p* values 0.0143, >0.9999, >0.999, 0.390, PLP1 overall $p = 0.0111$, individual *p* values 0.1836, 0.0348, >0.9999, 0.0724. For Figure 7*b*, statistics are one-way ANOVA, Bonferroni *post hoc* test, sample size = 5, and *p* values 0.0086, 0.00072, 0.0063. For the *in vitro* data in Figure 5*c*, there are 7–10 cells per group; and the entire branching distribution is shown, with no statistical comparison. For Figure 7*d*, there are five samples per group, one-way ANOVA, Bonferroni *post hoc* test, and *p* values are 0.0061, 0.0372. For the *in vivo* behavioral data (see Fig. 7*e*), statistics are two-way ANOVA, sample size is 8 or 9 per group, *p* values are 0.0008, 0.0761. For Figure 5, statistics are two-way ANOVA, sample size is 8 or 9 per group, and *p* values are 0.0008, 0.0761. For the tissue analysis after Matrilin-2 delivery in aged white matter stroke (see Fig. 9), sample size is 8 or 9 per group (see Fig. 9*a*,*b*), and $p = 0.00066$ and $p = 0.037$. In g ratio calculations (see Fig. 9*c*,*d*), there are 5 animals per group, at least 100 axons measured per animal ($p = 0.0003$, two-tailed *t* test).

Results

OPC transcriptome

Subcortical white matter stroke induces proliferation and accumulation of OPCs around the lesion site but very limited differentiation of these OPCs into mature OLs (Sozmen et al., 2016). The peak of proliferation of OPCs after white matter stroke is day 5, and the peak of limited differentiation of these OPCs into cells with markers of mature OLs is day 15 after white matter stroke (Sozmen et al., 2016). These two time points were taken as proliferation and limited differentiation time points in these studies. LCM was used to isolate the OPCs in the border of the stroke lesion, where axons are preserved but OPC differentiation is blocked (Sozmen et al., 2016) (Fig. 1*a*,*b*). This approach was taken, instead of an approach, such as single-cell RNAseq, so as to spatially localize OPC capture for transcriptional profiling, allowing specific isolation of OPCs in the region of white matter adjacent to the stroke or lesion site, with damaged or demyelinated axons. OPCs were labeled with lentivirus with a PDGFRα promoter driving membrane-bound lck-GFP (Fig. 1*c*,*d*) and captured within white matter 200 μm of the infarct at the peak of the OPC proliferation after white matter stroke (5 d after stroke) and at the time point of very limited differentiation of these cells (15 d) (Sozmen et al., 2016); and in control (nonstroke) white matter from the same subcortical white matter region; 300–400 cells in 8 sections per animal were captured for RNA analysis.

Isolated total RNA was amplified and deeply sequenced in 10 samples for day 5, day 15, and control. Quality control was performed after the alignment to examine the following: the level of mismatch rate, mapping rate to the whole genome, repeats, chromosomes, and key transcriptomic regions (exons, introns, UTRs, genes). Samples from 5 animals failed quality control and were excluded from further analyses (2 in day 5 and 3 in day 15). Between 65% and 81% of the reads mapped uniquely to the mouse genome. Across the samples, ~25% of the annotated genes were detected by at least 50 reads. Only genes with an FDR of < 0.1 were further analyzed. To determine the specificity of this approach to OPCs in white matter stroke, the differentially regulated genes at day 5 and day 15 in stroke OPCs and control were assessed for the top astrocyte, neuronal, and microglial markers (Thomas et al., 2006; Cahoy et al., 2008; Zamanian et al., 2012; Zhang et al., 2014). This analysis indicates that the RNAseq data are largely OPC-specific, with a possible minor contamination of microglia (Fig. 1*e*).

Within FDR < 0.1, unsupervised clustering of the expression profile by sample according to the highest total gene read counts indicates that samples from each time point clustered together, with the exception of one day 5 sample, which was an outlier, and one day 15 sample which clustered with day 5 (Fig. 2*a*). The clustering data and differential expression analysis indicate that the stroke OPC transcriptome is largely distinct from control, nonstroke OPCs, and distinct yet again across the early, proliferative and late, limited-differentiating time points in white matter stroke.

A comparison of the differentially expressed genes in stroke OPCs from proliferating day 5 OPCs to limited regenerating day 15 OPCs may provide insight into how these progenitors evolve in their response to stroke. At FDR < 0.1, 439 genes are differentially expressed in proliferating day 5 stroke OPCs compared with control OPCs. A total of 1695 genes are differentially expressed in the limited regenerating day 15 stroke OPCs compared with control OPCs. A total of 462 genes are differentially expressed from day 5 to day 15 (Fig. 2*b*; Table 1-1, available at https://doi.org/10.1523/JNEUROSCI.0103-19.2019.t1-1). qPCR of selected genes identified in the RNAseq studies confirmed that 22 of 25 genes had similarly significant changes in gene expression from RNAseq to qPCR (Fig. 3*b*).

To understand how proliferating (day 5) and limited-regenerating (day 15) OPCs compare in their transcriptome to OPCs in control conditions, these mouse white matter stroke OPC transcriptomes were compared with the most comprehensive database of mouse OL lineage cells (Zhang et al., 2014). There is a small overlap of early (day 5) and late (day 15) stroke OL lineage transcriptomes with control adult OPC and OL transcriptomes (Fig. 2*c*,*d*). However, there is little difference in the percentage of the stroke OPC transcriptomes at days 5 and 15 that overlap with published gene sets from mature OL transcriptomes, indicating that there is not a progressive expression of mature OL genes over time after white matter stroke. In addition

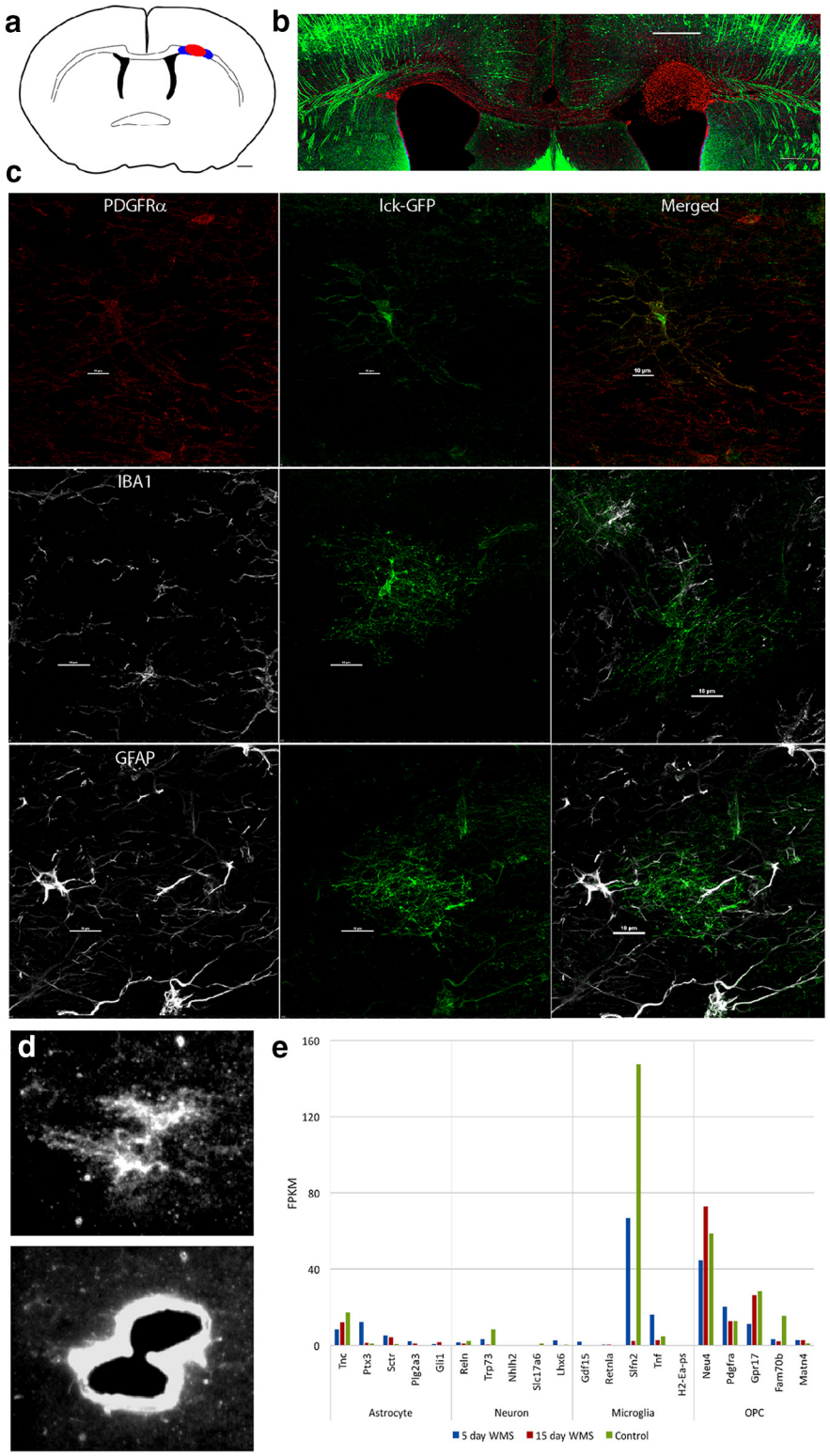

Figure 1. White matter stroke and LCM. ***a***, Schematic of location of white matter stroke (red) in coronal section of mouse brain. Blue areas represent regions of LCM of OPCs. Scale bar, 500 μm. ***b***, White matter stroke in YFP-H mouse in which layer 5 neurons are densely labeled. The red cells are DAPI stains, with pseudocolor to red for visualization. Scale bar, 300 μm. ***c***, The specificity of the viral labeling of OPCs (Ick-GFP) in white matter is shown with coimmunohistochemical staining for markers of microglia (IBA1), astrocytes (GFAP), and OPCs (PDGFRα). Scale bar, 50 μm. ***d***, Viral labeling of OPC and then laser dissection of OPC for downstream RNA isolation and sequencing. Lentivirus with membrane-bound GFP (Ick-GFP) under the control of the PDGFRα promoter is injected into the white matter adjacent to the stroke (***a***, blue region), labeling OPCs. These are microdissected in the region of partial damage to white matter, adjacent to the stroke site. ***e***, To assess the OPC specificity of the RNAseq dataset, fragments per kilobase of transcript per million reads mapped (FPKM) data for each of the three treatment groups were compared with the most cell type-specific genes identified in an online database (Zhang et al., 2014). FPKM values for the top 10 most cell type-specific genes of the indicated type cell type are compared with the day 5 and day 15 regenerating OPCs transcriptomes in white matter stroke.

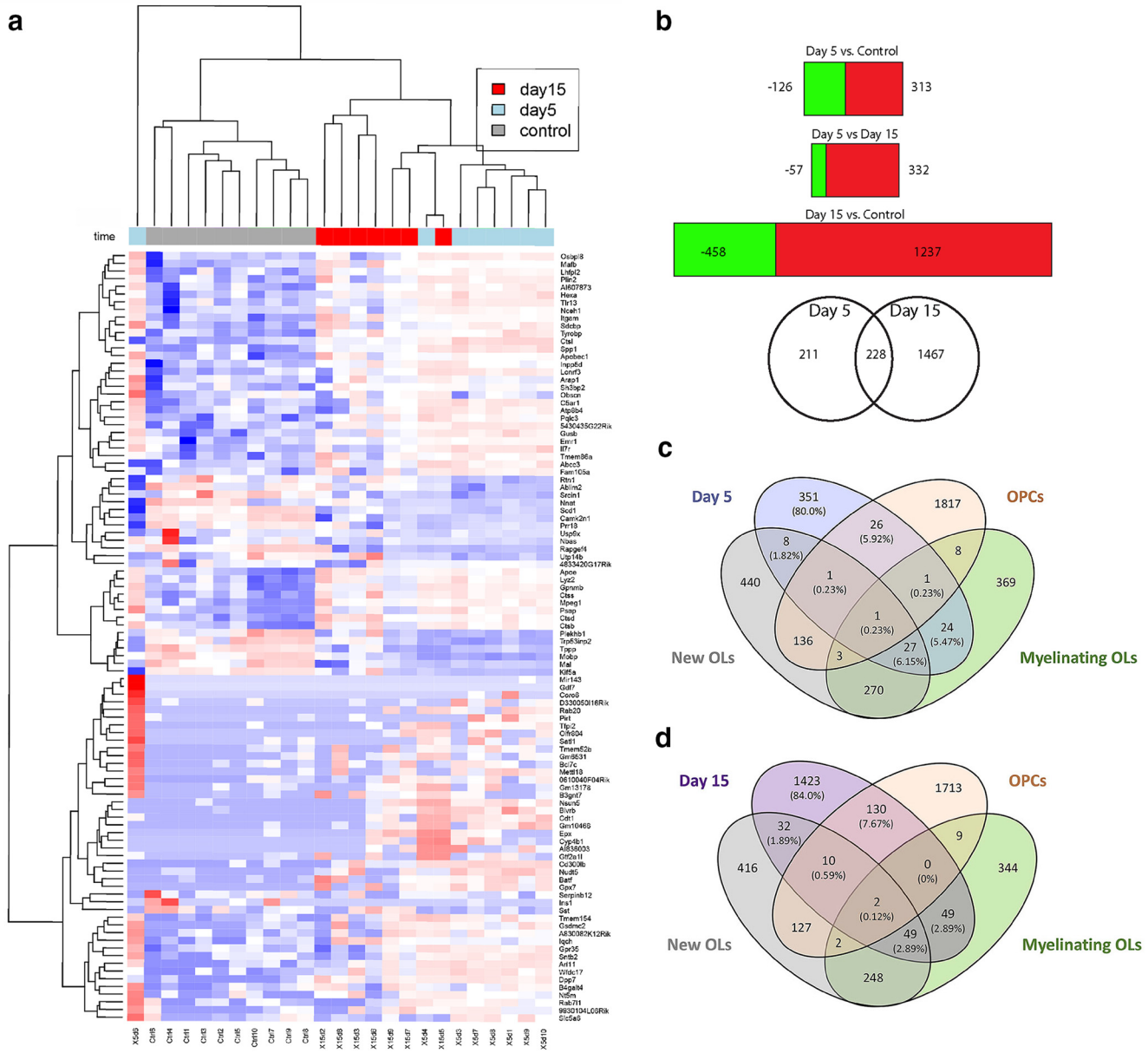

Figure 2. Transcriptional profile of OPCs responding to white matter stroke. ***a***, Unsupervised clustering of the top 100 genes with highest total gene read counts and differential expression at FDR threshold 0.1 in any comparison. Blue to red represents low to high values (scaled for each row). The 5 and 15 d stroke OPC transcriptomes cluster together and away from the control (nonstroke) OPC transcriptome, except for overlap of 2 cases, indicating that the OPC transcriptional response after stroke is a distinct molecular profile compared with nonstroke OPCs, and is different over time after stroke. ***b***, Differentially expressed genes across comparisons with FDR < 0.1. Green represents downregulated and red represents upregulated for each corresponding condition Venn diagram of differentially expressed genes in day 5 and day 15. The differentially expressed genes are listed in Table 1-1 (available at https://doi.org/10.1523/JNEUROSCI.0103-19.2019.t1-1). ***c***, ***d***, Comparison of stroke OPC transcriptomes at day 5 and 15 with published transcriptomes from OLs and OPCs (Zhang et al., 2014). There is not substantial overlap of the 5 d stroke OPC transcriptomes with control (nonstroke) OPCs, new oligos, or myelinating oligos and that that that this overlap does not increase, even with time and the limited differentiation that occurs in OPC after stroke, as seen in the 15 d stroke OPC transcriptome. Additional comparisons to published OPC transcriptomes are in Table 1-2 (available at https://doi.org/10.1523/JNEUROSCI.0103-19.2019.t1-2).

to the Zhang et al. (2014) RNAseq database, these stroke OPC transcriptomes were statistically compared with the other available OPC or OL gene expression profiles (Table 1-2, available at https://doi.org/10.1523/JNEUROSCI.0103-19.2019.t1-2). There is no difference in the percentage of the stroke OPC transcriptomes at days 5 and 15 that overlap with published gene sets from mature rat and mouse OL transcriptomes (Nielsen et al., 2006; Cahoy et al., 2008), supporting the observation that OPCs over time after stroke are expressing genes distinct from those characteristic of a maturation pathway. A comparison of reactive OPCs in white matter stroke to human white matter or cortical OPCs (Auvergne et al., 2013) shows that day 5 and day 15 transcriptomes overlap significantly only with human white matter OPCs but not cortical OPCs (Table 1-2, available at https://doi.org/10.1523/JNEUROSCI.0103-19.2019.t1-2). These data indicate, compared with control OPCs, OPCs after stroke differentially regulate more genes in the limited differentiation than the proliferative phase and exhibit a distinct transcriptional profile that does not evolve over time to resemble mature OLs.

The proliferating day 5 and limited regenerating day 15 stroke OPC transcriptomes contain distinct canonical signaling systems that are significantly regulated across time points after stroke (Table 1). For example, the canonical pathways that are active in day 5 stroke OPCs involve retinoic acid and other nuclear recep-

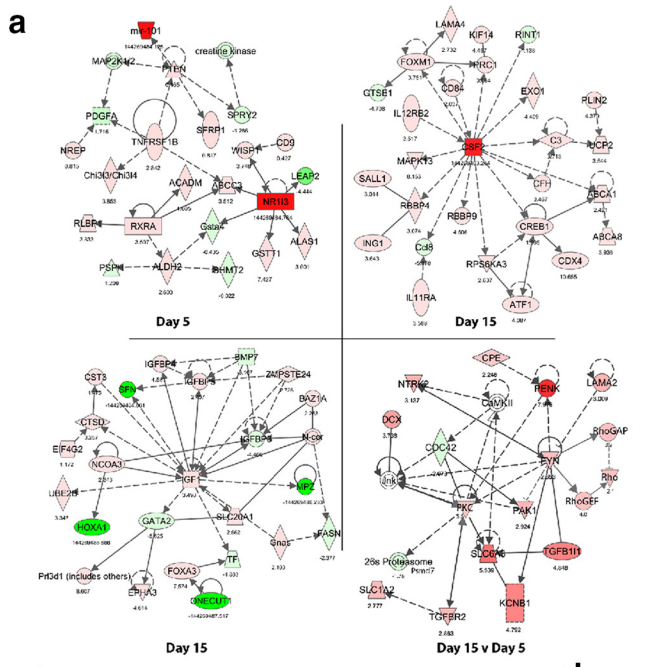

b

Gene	5d PCR	p val 5d PCR	15d PCR	p val 15d PCR	5d/15d
GDF7	20.200	1.09E-04	3.480	0.266	5.804598
Coro6	11.600	1.36E-04	-1.667	0.244	6.958608
fzd9	19.000	1.39E-04	24.100	2.60E-05	0.788382
FGF15	17.000	2.04E-04	1.800	0.636	9.444444
Matn2	13.400	0.001	-2.500	0.020	5.36
Ccr7	-4.000	0.001	2.600	0.017	1.538462
Adora2a	-8.400	0.001	-6.420	0.001	1.308411
BMP3	-5.400	0.002	-3.710	0.001	1.455526
GDF3	5.700	0.003	2.170	0.120	2.626728
fyn	-0.600	0.025	4.900	0.009	0.122449
Figf	-3.700	0.046	-18.270	4.78E-05	0.202518
inhbA 2	-5.500	0.162	-2.640	0.415	2.083333
Pou2F1	1.300	0.248	2.000	0.202	0.65
Rhoc	4.500	0.250	3.500	4.53E-04	1.285714
Rxra	3.400	0.260	3.600	0.002	0.944444
HBEGF	-3.300	0.277	-5.410	0.002	0.609982
Hes5	-2.100	0.277	2.460	0.233	0.853659
Cxcl13	2.100	0.400	42.000	4.95E-05	0.05
Bex4	-1.300	0.410	-13.590	3.90E-05	0.095659
BMP7	-4.200	0.481	-2.240	0.001	1.875
GPC6	-2.500	0.606	8.400	2.57E-04	0.297619
Lingo 1	1.000	0.606	1.300	0.606	0.769231
Notch1	-4.700	0.638	-3.000	0.004	1.566667
GDF11	-4.330	0.678	-2.000	0.001	2.165
TGFRB3	0.700	0.769	1.800	0.993	0.388889

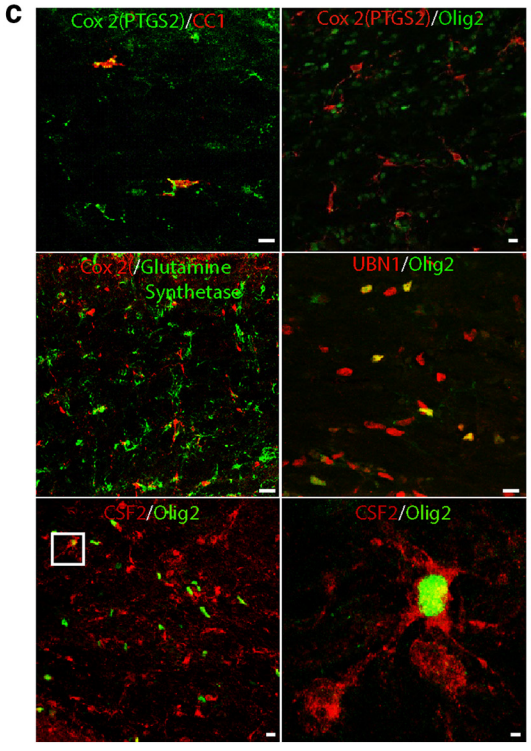

d

Day 5			Day 15			Day 5 vs Day 15		
Upstream Regulator	Activation z-score	P-value	Upstream Regulator	Activation z-score	P-value	Upstream Regulator	Activation z-score	P-value
IL6	2.934	7.56E-03	SPI1	3.13	2.08E-06	CEBPE	2.20	3.480E-03
PI3K (complex)	2.747	2.44E-02	IL6	2.934	7.13E-03	IFNA2	2.20	4.620E-01
STAT3	2.555	6.05E-02	TNF	2.797	7.14E-05	POR	2.18	1.050E-01
LDL	2.416	1.46E-01	MYD88	2.629	1.46E-02	FADD	2.16	4.220E-01
SPI1	2.415	2.08E-06	LDL	2.416	1.27E-01	LDLR	2.07	4.510E-02
OLR1	2.412	6.67E-03	OLR1	2.412	6.67E-03	IL2	2.06	6.130E-02
CSF1	2.407	1.49E-04	ETS1	2.313	6.94E-02	PGR	2.00	1.670E-01
mir-223	2.324	1.93E-08	TLR4	2.313	1.31E-02	DDX58	2.00	3.140E-01
CTGF	2.2	3.54E-01	Cg	2.245	2.62E-02	EIF2AK2	2.00	4.360E-01
ESR1	2.118	3.49E-02	IFNG	2.221	3.26E-04	NR1H4	2.00	2.210E-01
TGFBR2	2.059	6.83E-02	CTGF	2.2	3.13E-01	SMARCA4	1.98	1.950E-01
OSM	1.994	4.54E-01	CEBPE	2.2	3.48E-03	NR5A2	1.93	4.220E-01
DMD	1.951	5.31E-03	FADD	2.159	4.22E-01	IRF8	1.92	1.000E+00
C5	1.949	2.23E-01	ESR1	2.04	3.49E-02	P38 MAPK	1.90	8.270E-02
NOS2	1.943	3.79E-01	INHA	2.04	4.54E-03	IL1A	1.76	9.630E-02
IL12 (complex)	1.912	6.60E-02	PGR	2	1.54E-01	MYD88	1.68	1.460E-02
IL18	1.909	1.00E+00	HRG	2	6.55E-02	ESR1	1.57	3.490E-02
IKBKG	1.873	7.90E-02	BID	2	1.55E-02	INHA	1.54	4.540E-03
IKBKB	1.853	7.12E-02	OSM	1.994	4.54E-01	mir-135	1.39	6.550E-05
SMAD3	1.677	2.13E-02	NR4A1	1.982	2.42E-01	SPI1	1.34	2.080E-06
CHUK	1.615	2.78E-02	WNT1	1.982	7.46E-02	STAT5a/b	1.34	4.030E-02
IFNB1	1.6	7.24E-03	TP53	1.977	5.31E-05	STAT1	1.27	3.010E-03
HTT	1.595	1.97E-02	CCR5	1.965	1.41E-01	CSF3	1.23	2.570E-03
FIGLA	1.572	3.66E-02	TNFSF12	1.944	6.48E-03	WT1	1.21	4.240E-02
CD44	1.521	3.42E-03	CSF2	1.942	4.97E-06	Hdac	1.10	7.110E-05
STAT1	1.472	3.01E-03	NR5A2	1.929	4.22E-01	TBX21	1.07	9.180E-03
MAP2K1/2	1.432	1.39E-02	IRF8	1.92	1.00E+00	SMARCA2	1.07	4.260E-02
MYD88	1.392	1.46E-02	P38 MAPK	1.9	7.53E-02	IRF2	1.03	9.730E-03
TNFSF12	1.376	1.26E-02	IL1A	1.897	9.63E-02	TP53	1.02	5.310E-05

Figure 3. Analysis of stroke OPC transcriptome. ***a***, Molecular pathway analysis of differentially regulated genes in 5 d, 15 d, 15 d versus 5 d stroke OPC transcriptomes. All genes are FDR ≤ 0.1. Red represents upregulation. Green represents downregulation. The fold change (log2) for each gene is indicated below the gene symbol. Several genes are hubs in their links within these networks, such as RXRa and PTEN in day 5, CSF2, and IGF1 in day 15, and Fyn and PKC in day 15 versus day 5. Dotted lines indicate indirect relationship, in which an association is reported in the literature but not a mechanistic role. ***b***, Confirmatory qPCR analysis of select differentially regulated genes from RNAseq dataset of 5 and 15 d stroke OPC transcriptomes; 5 and 15 d qPCR columns show fold change relative to expression of that gene in control (nonstroke) subcortical white matter OPCs. *p* value columns are two-tailed *t* test comparisons between 5 or 15 d versus control. ***c***, Immunohistochemical staining for Cox2 (PTGS1), UBN1, and CSF2 15 d after stroke. Cox2 colocalization with markers of OL-lineage cells (Olig2) and mature OLs (CC1) and Cox2 colocalization with a marker of mature astrocytes (glutamine synthetase). UBN1 colocalization with Olig2. CSF2/Olig 2 and overlap in the same microscopic field. The box in the overlap image is enlarged in the rightmost panel. Scale bar, 20 μm. ***d***, List of most significantly associated upstream regulators that are predicted to induce genes in the day 5 and day 15 OPC stroke transcriptomes, and that would induce genes that are significantly different in day 5 to day 15. *p* value is Fisher's exact test and indicates that a given upstream regulators has a significant predicted interaction with the transcriptome. The activation score indicates the strength of the induction or inhibition of a set of downstream genes from a particular upstream regulator.

tor signaling (5 pathways), p38/MAPK signaling, proteoglycan degradation, fatty acid and cholesterol synthesis (involved in membrane and myelin production), and ECM turnover pathways. This is consistent with active proliferation/differentiation at day 5. Interestingly, one of the genes with the greatest differential expression between day 5 compared with day 15 is Matrilin-2 (Fig. 3*b*; Table 1-1, available at https://doi.org/10.1523/JNEUROSCI.0103-19.2019.t1-1), with an RNAseq log2 fold

Table 1. Canonical pathways significantly regulated in stroke OPCs

Day 5	Day 15	Day 5 to Day 15
LXR/RXR activation‡	IL-12 signaling**	HGF signaling†
PXR/RXR activation‡	Role of IL-17F in inflammatory airway diseases**	GPCR signaling
Neuroprotective role of THOP1 in Alzheimer's disease	Role of pattern recognition receptors in bacteria and viruses**	LPS-stimulated MAPK signaling**
Hepatic cholestasis	GPCR signaling	Prostanoid biosynthesis
VDR/RXR activation‡	FLT3 signaling in hematopoietic progenitor cells	IL-12 signaling and production in macrophages**
LPS/IL-1 mediated inhibition of RXR function	Fcγ receptor-mediated phagocytosis in macrophages**	CD28 signaling in T helper cells**
TR/RXR activation‡	VDR/RXR activation‡	14 –3-3-mediated signaling
Oleate biosynthesis††	Reelin signaling in neurons	Erythropoietin signaling
P38 MAPK signaling	cAMP-mediated signaling	Macropinocytosis signaling
Complement system	Production of reactive oxygen species in macrophages	Renal cell carcinoma signaling
Coagulation system	Molecular mechanisms of cancer	Protein kinase A signaling
Chondroitin sulfate degradation*	LXR/RXR activation‡	Glioma signaling
Visual cycle	T helper cell differentiation**	P2Y purigenic receptor signaling pathway
Dermatan sulfate degradation*	Factors promoting cardiogenesis	IL-3 signaling**
Parkinson's signaling	p38 MAPK signaling	Prolactin signaling
Epoxysqualene synthesis††	MSP-RON signaling pathway	PI3K signaling in B lymphocytes**
Palmitate biosynthesis††	Hepatic fibrosis/hepatic stellate cell activation	Huntington's disease signaling
Fatty acid biosynthesis initiation††	LPS-stimulated MAPK signaling**	Breast cancer regulation by stathmin1
Threonine degradation	EGF signaling†	Role of IL-17A in arthritis**
Granulocyte adhesion and diapedesis	NF-κB signaling**	VDR/RXR activation‡
Glutathione redox reactions	Dendritic cell maturation**	Glucocorticoid receptor signaling**
PPARα/RXRα activation‡	TREM1 signaling**	Regulation of IL-2 expression in activated and anergic T lymphocytes**
cAMP-mediated signaling	FGF signaling†	Inhibition of angiogenesis by TSP1
Type I diabetes mellitus signaling	Neurotrophin/TRK signaling†	Pancreatic adenocarcinoma signaling
Oct4 in ES pluripotency	PI3K signaling in B lymphocytes**	NF-κB signaling**

*ECM turnover.

**Inflammatory signaling.

†Growth factor signaling.

††Fatty acid/cholesterol metabolism.

‡Nuclear receptor signaling.

change of −11 (2100-fold downregulated at day 15) and a qPCR change from 13.4 fold upregulated at day 5 and −2.5× downregulated at day 15. Matrilin-2 is an ECM protein with a role in peripheral nerve regeneration (Malin et al., 2009). These signaling pathways have been implicated in OPC responses to nonstroke injury, particularly retinoid acid receptor function (Huang et al., 2011a), and in myelin formation (Kidd and Trapp, 2010). The canonical pathways that are active in day 15 stroke OPCs continue to reflect retinoic acid signaling (2 pathways) but also heavily involve inflammatory (12 pathways) and growth factor signaling (3 pathways).

We analyzed the day 5 and day 15 stroke OPC transcriptomes to determine whether specific signaling pathways are coordinately regulated in OPCs at these time points after stroke. Stroke regulates signaling systems related to RXRa and PTEN, two gene systems that play a role in OPC differentiation in nonstroke demyelinating white matter lesions (Huang et al., 2011a; González-Fernández et al., 2018) at proliferating day 5. At day 15, stroke differentially regulates several gene systems with roles in OPC differentiation or the tissue response to injury: colony stimulating factor 2 (CSF2), IGF-1, CREB, TLR4, STAT 4 and 6, and p38/MAPK (Fig. 3*a*; Table 1-1, available at https://doi.org/10.1523/JNEUROSCI.0103-19.2019.t1-1). In the genes that are significantly regulated at day 15 compared with day 5, the differential regulation of Rho, RhoGEF, and RhoGAPs, cdc 42, and Fyn corresponds to a downstream signaling system common to many axonal growth inhibitors, including the NgR1/LINGO-1 complex (Schmandke et al., 2007; Montani et al., 2009), which plays a key role in limiting OPC differentiation after white matter stroke (Sozmen et al., 2016). Several of these gene products have been more closely associated with cells other than OPCs/OLs, but immunohistochemical staining shows colocalization with OPC and OLs after white matter stroke for several of these proteins, including cyclooxygenase 2 (Cox2/PTGS2), ubinuclein 1 (UBN1), and CSF2 (Fig. 3*c*), suggesting that OPCs may take on novel roles poststroke. Fyn expression peaks in OPCs during developmental myelination, and its signaling systems modulate Rho to control morphological maturation of OPCs and MBP expression (White and Krämer-Albers, 2014).

We next investigated which transcriptional regulators might control differential gene expression in stroke OPCs. Day 5 and day 15 transcriptomes were analyzed for upstream regulators: molecules that induce or downregulate expression in a specific group of genes that are regulated in the OPC transcriptomes (Fig. 3*d*). Predicted transcriptional regulators were analyzed by significant association with differentially induced genes in each transcriptome, using a Fisher's exact test in which a p value indicates that a given upstream regulator has a significant predicted interaction with the transcriptome. Additionally, an activation score was assessed, indicating the strength of the induction or inhibition of a set of downstream genes from a particular upstream regulator. Both values rank the strength of an association of an upstream regulator with a predicted effect on the gene expression profile in OPCs as they respond to white matter stroke stroke in early, proliferative and later limited regenerative phases. The upstream regulators differ by time point in stroke OPCs and include immune cytokines, such as IL-3, IL-4, IL-10, IL-13, and TNF. Most of these upstream regulators produce gene expression changes that are seen in stroke OPCs, but these molecules themselves are not differentially expressed in stroke OPCs, implying a cell nonautonomous role. Inhibin A is one of the extrinsic transcriptional regulators with the highest activation score when

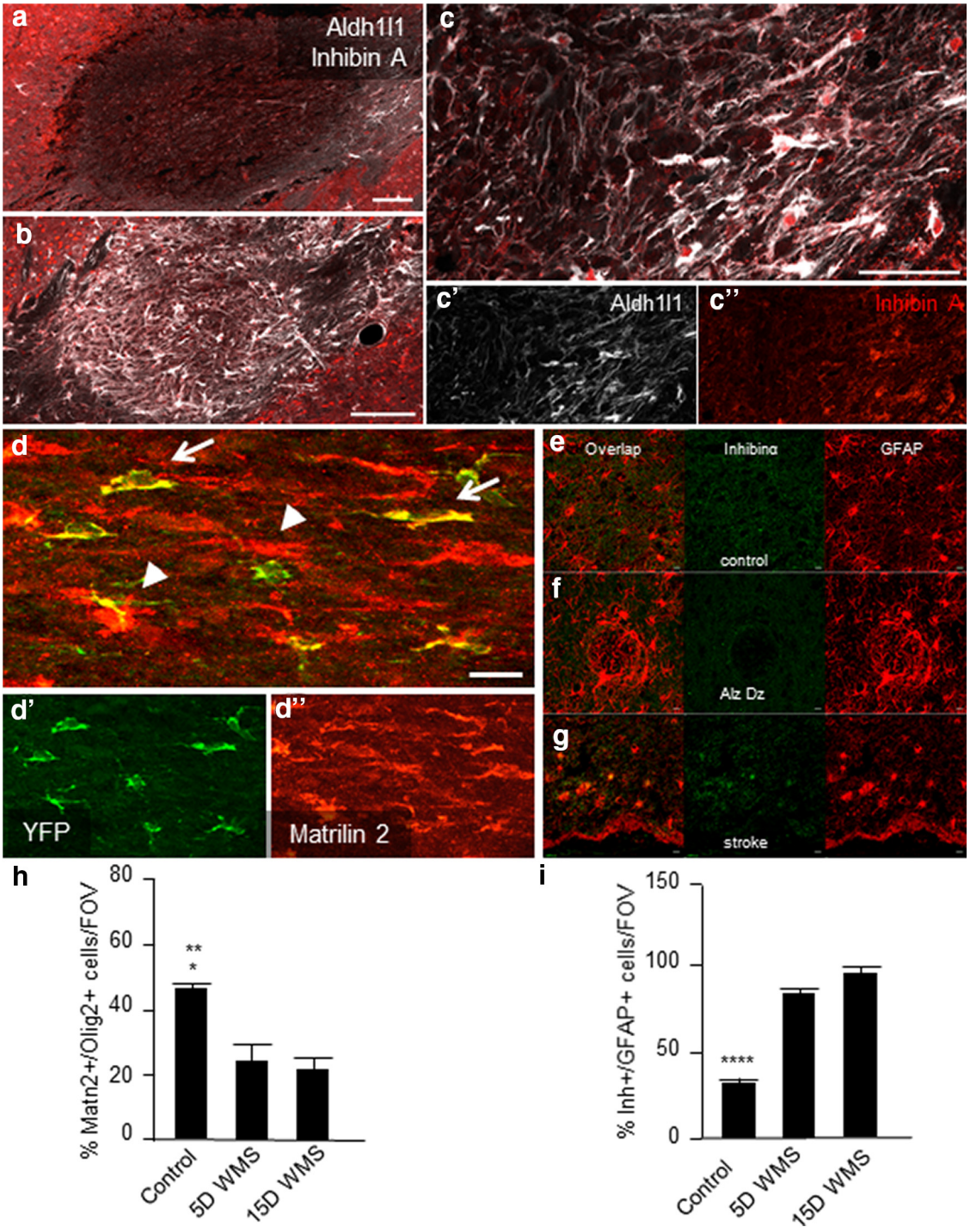

Figure 4. Astrocyte and OL/OPC Matrillin-2 and Inhibin A signaling. ***a–c***, Inhibin A subunit Inhibinα is used as a marker to compare tissue levels of the growth factor (red), Aldh1l1 (white) labels astrocytes. At 5 d after lesion (***a***), there is no detectable Inhibinα signal within the stroke, whereas labeling of 15 d stroke sections (***b***) revealed high levels of Inhibinα^+ cells filling the lesion. In higher magnification, at the edge of the stroke. ***c–c''***, The majority of Inhibinα label colocalizes with Aldh1l1$^+$ astrocytes shown in higher magnification. Inhibinα (red) and Aldh1l1 immunohistochemistry 5 d after stroke (***a***) and 15 d after stroke (***b***). ***c***, Higher magnification shows colocalization of Aldh1l1 staining with inhibinα. Scale bars: ***a–c***, 100 μm; ***c'***, 20 μm. ***d***, In a NG2-CreERT2/r26YFP mouse, OPC reporter line 5 d after stroke. ***d'***, YFP$^+$ (yellow) OPCs colabel with ***d''***, Matrilin-2 (red) (arrows) in addition to other cell types (arrowheads). Scale bar, 100 μm. ***e–g***, Inhibinα staining in human white matter from control (***e***), Alzheimer's disease as a reactive astrocyte condition that is not stroke and in white matter stroke (***f***). Scale bar, 20 μm. ***h***, ***i***, Quantification of percent immunopositive staining for Matrilin-2 and Inhibinα in Olig2$^+$ cells in control and after stroke. *$p = 0.0111$ versus 5 d white matter stroke. **$p = 0.0040$ versus 15 d white matter stroke. ****$p < 0.0001$.

comparing day 15 with day 5 stroke datasets. Intriguingly, Inhibin A is reported as a repressor of Matrilin-2 expression (Nagaraja et al., 2010) (Fig. 3*d*).

In summary, RNAseq of OPCs in the reactive zone after white matter stroke shows that these cells display a dynamic gene expression profile distinct from resting OPCs, which changes over time as OPCs move from an early proliferative phase to one of limited differentiation. There is an initial activation of retinoic acid, fatty acid, and cholesterol synthesis pathways and later growth factor and inflammatory signaling systems. A coordi-

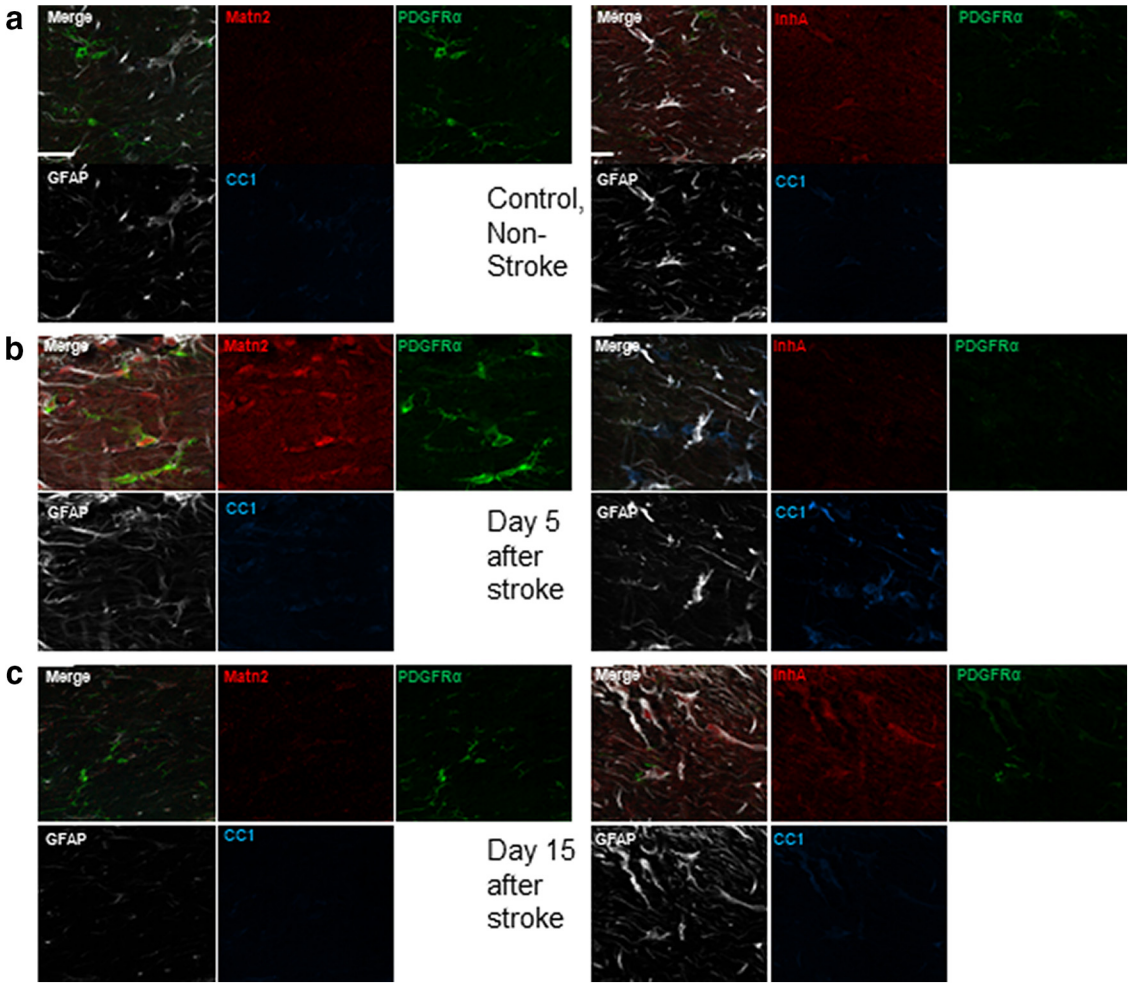

Figure 5. Matrilin-2 and Inhibin A immunofluorescence in white matter stroke. ***a***, Matrilin-2 (Matn2) and Inhibin α (InhA) immunofluorescence in control white matter, colocalized with makers of OPCs (PDGFRα), astrocytes (GFAP), and mature OLs (CC1). Matn2 and InhA levels are low in control white matter. ***b***, Matn2 staining is prominent 5 d after stroke and colocalizes extensively with PDGFRα. InhA staining remains low in 5 d after white matter stroke. ***c***, Matn2 staining is decreased to levels near control white matter at 15 d after stroke. InhA staining is increased and localizes with GFAP $^+$ cellular elements.

nated upregulation of Rho, RhoGEF, and RhoGAP family members and downregulation of CDC42 occur at day 15, which are downstream from NgR1. We have defined a role for NgR1 signaling in poststroke white matter repair (Sozmen et al., 2016). These data also highlight ECM turnover as an early pathway in the OPC response to white matter stroke. One such ECM protein, Matrilin-2, undergoes a dramatic induction and then inhibition in OPCs after white matter stroke, and an inhibitor for Matrilin-2, Inhibin A, is predicted to be active in white matter stroke by bioinformatic analysis of the day 5 versus day 15 transcriptomes.

Matrilin-2 and Inhibin relationship *in vitro* and *in vivo* in OPCs and white matter stroke

In line with the RNAseq and qPCR data, we found Matrilin-2 protein is increased in OPCs and in some astrocytes during the early phase of the disease, compared with the levels in control white matter (Figs. 4*a–d*,*h*, 5*a*,*b*). In contrast, at 15 d after stroke, few OPCs or other cells in white matter contained Matrilin-2, which is comparable with control white matter (Fig. 5*a*,*c*). Inhibin A exhibits an inverse profile following white matter stroke. At day 5, few cells in or near the infarct contain Inhibin followed by a dramatic increase in staining at day 15 in the edges of the infarct (Figs. 4*a–c*, 5*a*,*c*). At day 15, numerous astrocytes are positive for Inhibin in the center of the stroke core and in the peri-infarct white matter (Fig. 4*b*,*c*). This indicates that Inhibin is induced in astrocytes as the response to white matter stroke progresses and may activate receptors on OPCs. Previous research has identified Inhibins as binding to Activin receptors and competing with Activin signaling, through ActRIIa. Inhibin A may have a direct action via Inhibin binding protein/p120. Both ActRIIa and Inhibin binding protein/p120 are expressed in OPCs (Suresh et al., 2011) and were detected in OPC reporters or OLs (Fig. 6*a*,*b*). There is variance in the number of Olig2 $^+$ OL lineage cells that are immunopositive for these two receptors, and no significant change with white matter stroke (Fig. 6*c*,*d*). To investigate whether this signaling system was specific to the mouse model of white matter stroke, we also examined human stroke tissue. Inhibin is also induced in human white matter stroke (Fig. 4*e*) but not in nonischemic areas or in reactive astrocytes surrounding amyloid plaques in Alzheimer's disease (Fig. 4*e*).

To further investigate the effects of Matrilin-2 and Inhibin on OPC differentiation, we investigated their effects on primary OPC cultures. Matrilin-2 significantly induces expression of mature OL genes, such as Mobp and Plp1, while inhibiting expression of immature or progenitor genes, such as PDGFRα and NG2

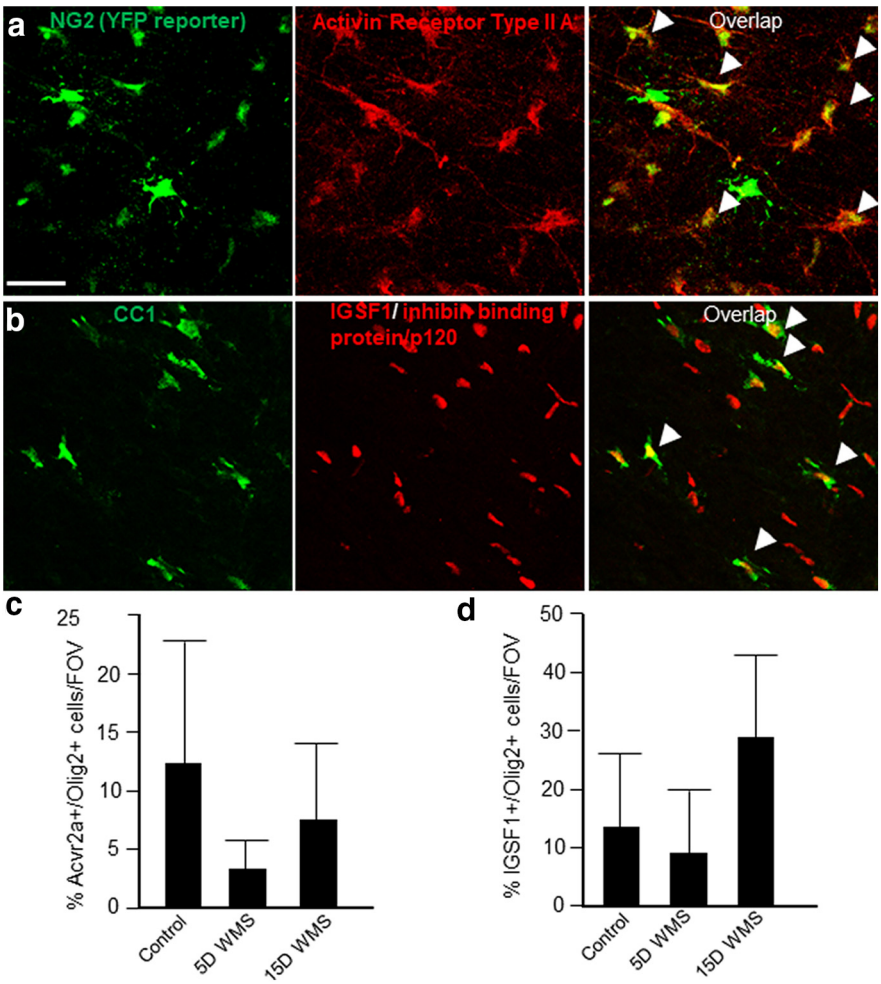

Figure 6. Colocalization of candidate Inhibin A receptors to OPCs or OLs. ***a***, OPC reporter mouse (NG2-CreERT2/R26 YFP) (Sozmen et al., 2016) and activin receptor IIa immunostaining. ***b***, Colocalization of the mature OL protein CC1 and Ig superfamily member 1 (IGSF1)/inhibin binding protein/p120. All photomicrographs taken at 7 d after stroke. Scale bar, 100 μm. ***c***, ***d***, Quantification of percent immunopositive staining for ActRIIa and IGSF-1 in Olig2$^+$ cells in control and after stroke. There is no statistically significant difference across conditions.

(Fig. 7*a*). As predicted from the upstream analysis of the OPC stroke transcriptome, Inhibin inhibits OPC expression of Matrilin-2 (Fig. 7*a*). When applied together to *in vitro* OPC cultures, Inhibin blocks the Matrilin-2-induced expression of the mature OL genes Mobp and Plp1 (Fig. 7*a*). In addition to gene expression studies, we looked at OL morphology, based on the observation that maturation leads to increased process length and complexity. We compared the extent of OL process growth and arborization in the presence of Inhibin and/or Matrilin-2 (Huang et al., 2011a; Rajasekharan et al., 2009) (Fig. 7*b*). Inhibin decreased the total number of processes, maintaining the cells in a simple morphology (PDL: 45.80 ± 11.12, PDL + Inhibin media: 9.67 ± 3.56, $p < 0.01$). In contrast Matrilin-2 increased the average number processes, indicating increased complexity of OL arbors, compared with growth of OPCS on PDL (standard cell culture) (Fig. 7*b*; PDL: 4.94 ± 1.05, PDL +; PDL + Matrilin-2: 19.13 ± 5.49, $p < 0.00001$; Fig. 7*b*,*c*). Matrilin-2 not only markedly increased the complexity of OLs ($p < 0.00001$; Fig. 7*b*,*c*); it also blocked the negative effects of Inhibin on OL process formation (Fig. 7*b*,*c*). The individual p values are, for Figure 7*a*, PDGFRα overall $p = 0.0002$, individual p values 0.0006, >0.9999, 0.0092, 0.9366, NG2 overall $p = 0.025$, individual p values 0.0118, >0.9999, 0.0043, >0.9999, MOBP overall $p = 0.0141$, individual p values 0.0143, >0.9999, >0.999, 0.390, PLP1 overall $p = 0.0111$, individual p values 0.1836, 0.0348, >0.9999, 0.0724. For Figure 7*b*, statistics are one-way ANOVA, Bonferroni *post hoc* test, sample size = 5, p values 0.0086, 0.00072, 0.0063.

Matrilin-2 did not alter the differentiation potential of OPCs (Fig. 7*d*). In contrast, Inhibin did affect differentiation, significantly decreasing the number of MBP$^+$ cells in culture (PDL: 45.5 ± 9.06%, PDL + Inhibin A media: 27.30 ± 5.44%, $p < 0.001$). There are five samples per group (one-way ANOVA, Bonferroni *post hoc* test, p values are 0.0061, 0.0372). This effect was attenuated when Matrilin-2 and Inhibin were both present in culture media. (Fig. 7*d*; 32.95 ± 6.34%, $p < 0.01$ relative to PDL control). In summary, soluble Matrilin-2 significantly promotes maturation of OLs, whereas Inhibin partially blocks Matrilin-2's prodifferentiation effect.

Matrilin-2 enhances functional recovery after white matter stroke

White matter stroke in humans produces profound deficits in movement control and gait (Whitman et al., 2001; Baezner et al., 2008; Soumaré et al., 2009) and is strongly age-associated (Iadecola, 2013). These motor deficits directly correlate with the development of cognitive impairments, vascular dementia, falls, and death (Verghese et al., 2002; Koo et al., 2012). To model movement deficits in the mouse, the use of aged mice is both

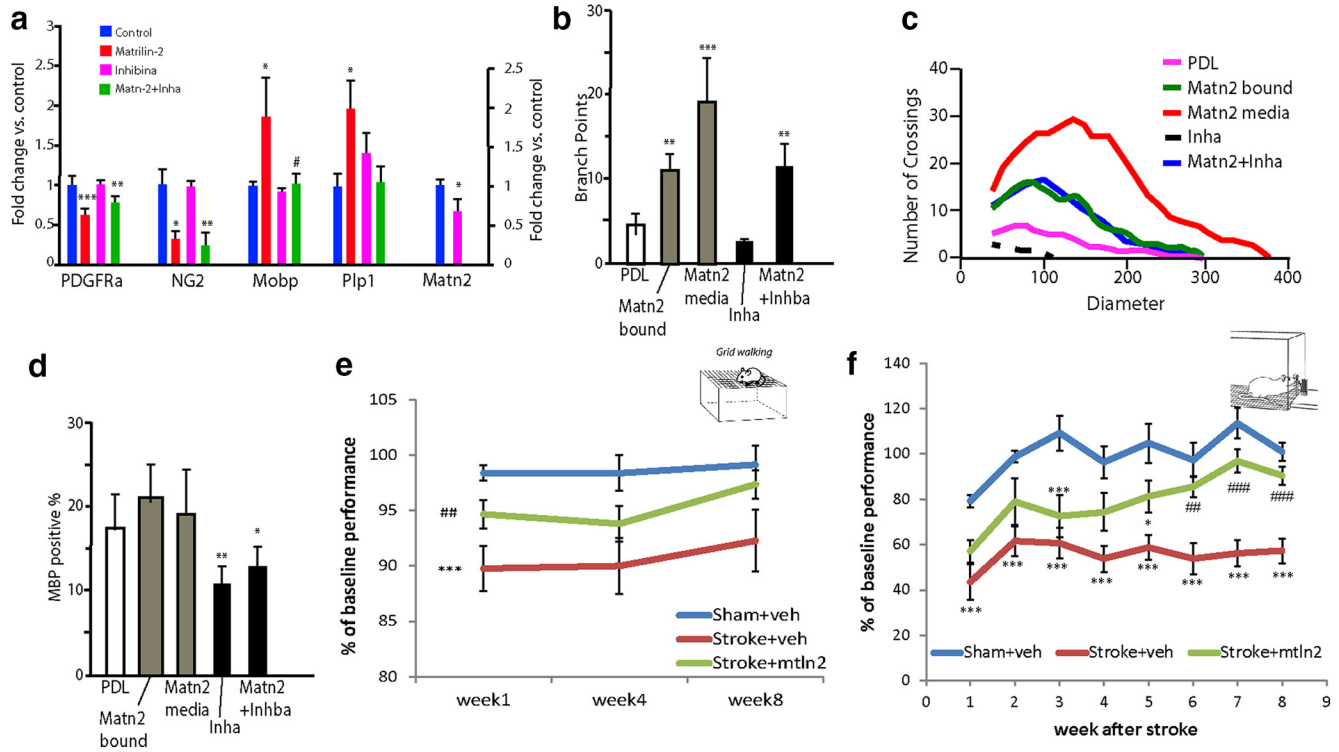

Figure 7. Matrilin-2 and Inhibin A *in vitro* and Matrilin-2 behavioral effects. ***a***, Primary OPC cultures exposed to control conditions, or Matrilin-2 (10 μg/ml) and inhibinα (10 μg/ml) and assessed with qPCR for mRNA levels of OPC (PDGFRα and NG2) and mature OL (Plp1, Mopb) markers. $^{***}p < 0.001$, $^{**}p < 0.01$, $^{*}p < 0.05$, versus control. $^{\#\#\#}p < 0.001$ versus Matrilin-2. ***b***, The number of crossings of OPC or OL branches, assessed by Sholl analysis. ***c***, The mean number of cell branches (*y* axis) at specific distances from the cell body (*x* axis) according to treatment condition. ***d***, Percentage of MBP$^+$ Olig2$^+$ double-labeled cells over the total number of Olig2$^+$ cells. $^{**}p < 0.01$, $^{*}p < 0.05$ versus control. ***e***, ***f***, Behavioral testing of aged animals. Aged mice ($n = 8$ per group) were injected with Matrilin-2 or vehicle 6 d after white matter stroke and functional testing was assessed via (***e***) grid-walking and (***f***) pasta handling tests. Results are presented as performance relative to prestroke baseline. $^{*}p < 0.05$, $^{***}p < 0.001$, compared with sham+veh. $^{\#\#}p < 0.01$, $^{\#\#\#}p < 0.001$, compared with stroke+vehicle (two-way ANOVA with Bonferroni *t* test pairwise comparisons).

clinically relevant and experimentally necessary, as young adult mice recover motor control within weeks of the stroke, whereas aged (20–22 months old) mice have persistent motor impairments in gait and skilled reaching (Rosenzweig and Carmichael, 2013). To test the effects of Matrilin-2 on measures of tissue repair after white matter stroke, this protein was injected into the boundary region of the stroke, in the site of injured axons and blocked OPC differentiation, 6 d after stroke (Fig. 1*a*) (Sozmen et al., 2016). Matrilin-2 persists for at least 7 d in the ECM around white matter stroke (data not shown). Aged mice received a stroke using the same technique as young adult male mice and either vehicle or Matrilin-2 was injected into the white matter adjacent to the stroke ($n = 8$ control, stroke+vehicle; $n = 9$ stroke+Matrilin-2). Motor control was measured in skilled use of the forelimb to grab individual pieces of pasta (pasta matrix task) (Rosenzweig and Carmichael, 2013) and in foot faults while walking on a challenging grid (grid-walking task) (Rosenzweig and Carmichael, 2013). Aged mice with stroke experience a deterioration in gait, seen as an increase in foot faults. This does not recover over 9 weeks after stroke. In contrast, mice with stroke+Matrilin-2 recover gait function significantly, beginning at 1 week after stroke (two-way ANOVA, difference of means = 7.958, $t = 5.257$, $p < 0.001$, Bonferroni) and at 9 weeks are not significantly different from control, no-stroke mice (two-way ANOVA, difference of means = 3.336, $t = 2.228$, $p < 0.076$, Bonferroni) (Fig. 7*e*). In the pasta matrix test, there is a slight drop-off in in performance in all groups, due to the time off from the surgery or the equivalent time gap in controls. Control mice quickly recover their performance. Stroke+vehicle mice never achieve >60% of their baseline performance. In contrast, stroke+Matrilin-2 mice are significantly better at skilled reach than stroke+vehicle at 5 weeks (two-way ANOVA, difference of means = 23.514, $t = 4.813$, $p < 0.037$, Bonferroni) after stroke and are not significantly different from control mice at 9 weeks (two-way ANOVA, difference of means = 10.626, $t = 1.114$, $p = 0.762$, Bonferroni) (Fig. 7*f*). These data indicate that local increases in Matrilin-2 after white matter stroke produce improved motor recover in this stroke subtype, in clinically relevant aged cohorts of mice.

Matrilin-2 promotes OPC differentiation and white matter repair *in vivo* after white matter stroke

To determine the effects of Matrilin-2 on tissue outcomes after white matter stroke, we measured OPC differentiation and myelin ultrastructure in control, stroke, and stroke+Matrilin-2, also using aged mice to understand the tissue effects that underlie behavioral recovery. OPC differentiation was quantified through immunohistochemical staining of Olig2, a marker of the OL lineage to the point of mature OLs (Huang et al., 2011a; Simon et al., 2011) and the mature OL marker, GSTpi (Simon et al., 2011). Cells in three states were quantified: immature OPCs (Olig2/GSTpi$^-$), intermediate maturation (Olig2/GSTpi$^+$), and a mature state (low or absent Olig2/GSTpi$^+$). This approach was validated in showing a significant association with morphological complexity of the OPCs as they mature, measured with viral cell filing *in vivo* with mCherry (Fig. 8*a*,*b*) and with virally tracked MBP expression (Fig. 8*c*,*d*). To measure OPC differentiation during a condition of Matrilin-2-stimulated behavioral recovery, tis-

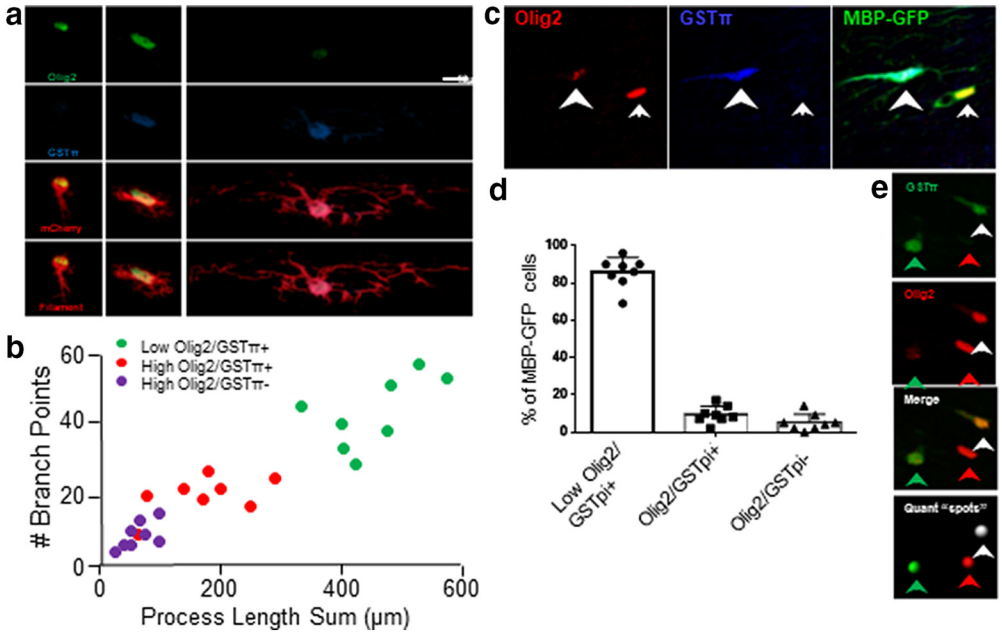

Figure 8. Validation of white matter OL quantification approach. Immunohistochemical staining for levels of Olig2 staining intensity (low/absent vs high) and presence or absence of the mature OL marker GSTpi was tested against other measures of OL morphology, including morphological complexity (***b***) and a marker of MBP expression (***c***). ***a***, Lentivirus with mCherry was injected using a dilute solution into subcortical white matter to fill sparse cells in the white matter with this fluorescent protein. The crossing points and number of branches were measured in Olig2/GSTpi-stained cells by segmenting the fully labeled cells as filaments (***a***, bottom) and quantifying brain points of these filaments per cell. ***b***, Quantification of Olig2/GSTpi measurements against cellular complexity as measured by branch points. Each dot represents quantification of one cell. Two cells were quantified per mouse, in 4 mice. The greatest arborization and complexity of cells are in the condition of low/absent Olig2 and GSTπ staining. ***c***, Lentivirus with GFP under the MBP promoter was injected into subcortical white matter. This labels cells with activation of the mature OL promoter MBP. The number of Olig2 high/low and GSTpi-expressing cells with GFP expression was quantified. Arrowhead indicates a cell with low Olig2/GSTpi$^+$. Arrow indicates a cell with high Olig2/GSTπ^-. ***d***, Quantification of percent of all pMBP-GFP$^+$ cells in subcortical white matter with distribution of Olig2 high/low-absent and GSTpi immunostaining by condition of GFP localization to these labeled cells. The morphologically mature, low olig2/GSTpi$^+$ OL population comprises >80% of MBP-GFP cells in subcortical white matter (682 cells in total from 8 sections). ***e***, To map the Olig2-GSTpi-labeled cells, OLs in the subcortical white matter were categorized into three spot objects: Olig2$^+$/GSTpi$^-$ cells (red arrow/spot), Olig2/GSTpi$^+$ cells (white arrow/spot), and low or absentOlig2/GSTpi$^+$ cells (green arrow/spot). ***f***, Quantification of OL lineages cells in white matter within 400 μm of stroke, as in Figure 6*b*, with each data point shown. Scale bars: (in ***a***, right) ***c***, ***e***, 10 μm.

sue sections from the aged cohorts of mice used in the behavioral studies were analyzed at study end, 9 weeks after stroke. OPC and mature OL number were digitally mapped in control, stroke+vehicle, and stroke+Matrilin-2 (Fig. 8*e*). Stroke causes an increase in total Olig2$^+$ cells and a loss of mature, low Olig2/GSTpi$^+$ cells (Fig. 9*a*,*b*). This is consistent with our previous reports of white matter stroke inducing a proliferation of Olig2$^+$ OPCs but a block in the differentiation of these progenitors into mature OLs (Sozmen et al., 2016). Stroke+Matrilin-2 significantly blunts the increase in Olig2$^+$ cells and increases the number of low Olig2/GSTpi$^+$ cells, markers of mature oligodendrocytes (Fig. 9*a*,*b*). Thus, in digital maps of the subcortical white matter near the infarct, Matrilin-2 induces more cells with markers of intermediate and mature OLs after stroke. To directly visualize myelin structure in aged mice with stroke+vehicle and stroke+Matrilin-2, separate cohorts were processed for electron microscopy of myelin profiles (stroke+vehicle and stroke+Matrilin-2, $n = 5$ each), and g ratio was measured in the corpus callosum medial to the stroke site at 9 weeks after stroke in stroke+vehicle and stroke+Matrilin-2. The g ratio is the ratio of the inner axonal diameter to the total outer diameter, a sensitive indicator of remyelination. Matrilin-2 promotes remyelination of axons adjacent to the infarct, seen as axons with significantly lower g ratios (Fig. 9*c*,*d*) (stroke+vehicle mean = 0.686, SD = 0.020; stroke+Matrilin-2 mean = 0.612, SD = 0.019, 5 animals per group, at least 100 axons measured per animal, $p = 0.0003$, two-tailed t test). Matrilin-2 delivery after stroke also increases the total percentage of axons adjacent to the stroke site that are myelinated (data not shown). These results indicate that Matrilin-2 enhances OPC differentiation and remyelination in the brain after subcortical white matter stroke.

Discussion

White matter stroke triggers a unique molecular profile within OPCs in the partially damaged tissue adjacent to stroke and in adjacent reactive astrocytes, which both initiate and limit tissue repair. Stroke induces OPCs to respond to the damage through proliferation, but these responsive OPCs have only a very limited differentiation into mature OLs (Sozmen et al., 2016). In this study, we report a unique OPC transcriptome specific to white matter stroke pathology. This dataset indicates that, in the proliferative phase of this OPC response, distinct molecular pathways are induced related to ECM remodeling, retinoic acid/nuclear receptors, PTEN signaling, and membrane biosynthesis. During the phase of limited differentiation, there is a marked upregulation of inflammatory signaling and growth factor pathways. One prominent gene that is highly induced during the proliferative phase of the OPC stroke transcriptome, and then significantly downregulated, is Matrilin-2, which codes for an ECM adapter protein associated with peripheral nerve regeneration. Analysis of the OPC stroke transcriptome for upstream regulators of this gene set and of Matrilin-2 identifies Inhibin A as a secreted molecule that is predicted to control expression of a significant number of genes in the OPC stroke transcriptome. Inhibin A is localized to reactive astrocytes in both mouse and human stroke, suggesting a poststroke glial signaling niche. Indeed, Matrilin-2 is initially upregulated in OPCs after stroke, until reactive astrocytes begin secreting Inhibin A, which down-

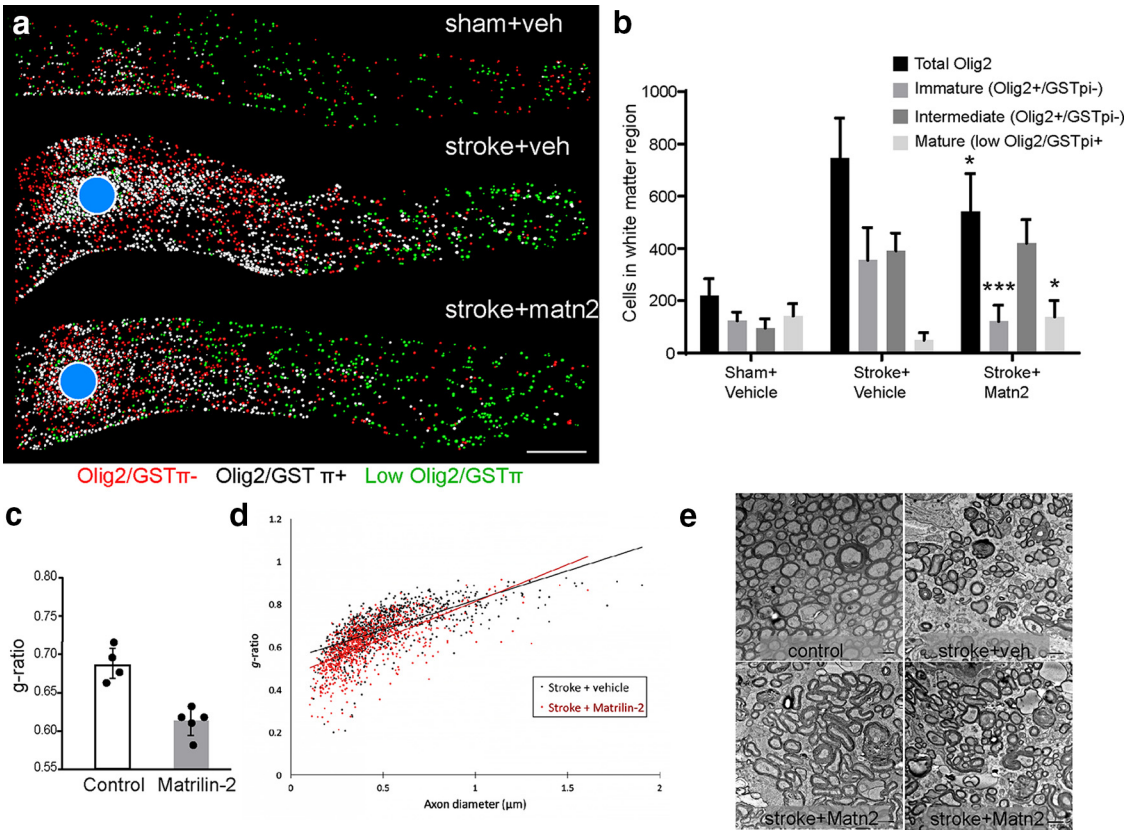

Figure 9. Matrilin-2 promotes tissue measures of OPC differentiation *in vivo*. ***a***, Distribution of OLs in the subcortical white matter was mapped 8 weeks after stroke. The number of spots in each category of mature OL (low olig2/GSTπ^+), intermediate OL (Olig2$^+$/GSTπ^+), and immature OL or OPC (Olig2/GSTπ^-) and their distance from the stroke lesion center (blue circles) mapped. Blue circle represents the center of the stroke. ***b***, Quantification of OL lineage cells in control, stroke, and stroke + Matrilin-2 delivery, 8 weeks after stroke. *$p < 0.05$ versus Stroke + veh. ***$p < 0.001$ versus Stroke + veh. ***c***, ***d***, G ratio was measured 9 weeks after stroke. The data are the mean g ratio for each animal ($n = 5$ for each group) ± SD. ***e***, Representative EM images from corpus callosum that were used to calculate g ratios, showing the different conditions in aged white matter, stroke, and two examples of exogenous matrilin-2 delivery.

regulates Matrilin-2 and may be part of the inability of OPCs to differentiate in this disease. *In vitro* studies confirm that Matrilin-2 induces, and Inhibin A opposes, OPC differentiation and that Inhibin A regulates Matrilin-2 expression in OPCs. *In vivo* studies show that Matrilin-2 promotes OPC differentiation and remyelination in white matter stroke and promotes behavioral recovery. These data identify an OPC-astrocyte niche that is triggered after white matter stroke and signals to inhibit tissue repair through in part an Inhibin/Matrilin-2 axis.

White matter stroke triggers an important interplay among astrocytes. Astrocytes are triggered into a reactive state over the course of the first 7 d after stroke in the region of initial OPC proliferation and later limited differentiation in white matter stroke. Further, a portion of the reactive (7%–13%) astrocytes bordering the lesion are actually derived from OPCs (Sozmen et al., 2016). This shunting of OPCs toward astrocytes instead of toward differentiated OLs in white matter stroke has been described in other diseases and cell culture (Raff et al., 1983; Barres et al., 1990; Zhu et al., 2008). In inflammatory and toxin-induced white matter injury, an astrocyte effect on OPC responses has been recently recognized. Astrocytes secrete or express on their surface a large number of molecules that either stimulate or block OPC differentiation (Barnett and Linington, 2013). There are no reported systems in oligo-astrocyte signaling in white matter stroke. Rather than work sequentially through the many astrocyte signaling systems identified in inflammatory or toxin injury to discover signaling systems in white matter stroke, we took a systems biology approach. We identified the transcriptional profile that is distinct between the proliferative phase of OPCs after stroke, and the phase of very limited differentiation into OLs. Among other gene systems, this approach identified Matrilin-2 as one of the most differentially regulated genes between the proliferation and limited-differentiation stages of OPCs after white matter stroke. We then predicted the molecules that could regulate this collection of genes, identifying candidate upstream regulators that themselves were not present in the two OPC stroke transcriptomes. A secreted factor with one of the highest *z* scores in this predicted set of upstream OPC regulators was Inhibin A, which has been reported to decrease the expression of Matrilin-2 (Skory et al., 2013).

Inhibins are dimers of α and β_A or β_B subunits originally described as antagonizing activin signaling in the anterior pituitary. There has been no described role for Inhibin A secretion and action within the brain. By tracking the specific subunit for Inhibin A, it is induced in reactive astrocytes at the margin of white matter stroke by 7 d after the infarct in the mouse white matter stroke model. Inhibin A is also induced in human white matter stroke in a specific manner, as it is not seen in reactive astrocytes in Alzheimer's disease. OPCs and OLs express Inhibin A receptors, although the receptor biology of Inhibin A is not well defined (Suresh et al., 2011). We confirm that Inhibin A reduces Matrilin-2 transcription in OPCs. Matrilin-2 stimulates differentiation of OPCs, and Inhibin A blocks differentiation of OPCs. The Inhibin A block to OPC differentiation can be partially overcome by Matrilin-2, suggesting that Matrilin-2 is downstream from Inhibin signaling in OPCs, as predicted. *In vivo* after white

matter stroke, Matrilin-2 promotes OPC differentiation, enhances remyelination of axons adjacent to the stroke, and promotes behavioral recovery. Matrilin-2 is an ECM adapter protein, which binds to and links together collagens and proteoglycans into a filamentous extracellular network. Matrilin-2 is active in muscle and liver regeneration (Korpos et al., 2015) and is also secreted by Schwann cells in peripheral nerve injury, promoting axonal regeneration. (Malin et al., 2009). Recently, Matrilin-2 has been implicated as an axonal signal in MS that stimulates macrophages (Jonas et al., 2014). These data identify Matrilin-2/Inhibin A as a new oligo-astrocyte signaling system in a glial niche within white matter stroke, which blocks OPC differentiation and recovery by inhibiting the ability of the OPC to modify the local ECM into a reparative state.

Bioinformatic analysis of the proliferative OPC stroke transcriptome and the limited differentiation OPC stroke transcriptome identifies other key molecular pathways that are active in each stage and predicted master regulators, which might control OPC responses. The downstream genes that are controlled by several classes of nuclear receptors are prominently regulated in the proliferative phase of OPC response after stroke. Five such pathways are activated: LXR/RXR, PXR/RXR, VDR/RXR, TR/RXR, and PPAR/RXR. Interestingly, these receptors themselves are not significantly altered in their gene expression levels in stroke OPCs, but many genes that are upregulated or downregulated at high statistical significance (FDR < 0.1) are regulated by these nuclear receptors These RXR nuclear receptors are from Type I and II classes and form homodimeric or heterodimeric pairings of a hormone-specific ligand element with a DNA binding element, which then control the expression of functionally related genes (Dawson and Xia, 2012). Changes in expression of nuclear receptors and their downstream genes are seen in OPC responses in toxin and inflammatory white matter lesions during OPC differentiation (Huang et al., 2011a), as opposed to stroke, where regulation of these genes occurs during the proliferative phase. RXRg has a causal role in OPC differentiation in MS models (Huang et al., 2011a). Nuclear receptors/RXR signaling promote differentiation, inhibit proliferation in cancers, and promote maturity in adaptive immune responses (Du et al., 2005; Dawson and Xia, 2012). The transcriptional data suggest that additional targets in nuclear receptor signaling systems may manipulate OPC differentiation in white matter stroke.

In the limited differentiation OPC stroke transcriptome 15 d after white matter stroke, a substantial number of inflammatory signaling pathways are present. These include 12 pathways that relate to intrinsic inflammation (Trem 1), or specific cytokine signaling pathways (IL-14, IL-12, and NF-κb). One of the defining features between the cellular responses to white matter stroke in young adult to those of aged mice is the greater activation of inflammation with age (Rosenzweig and Carmichael, 2013). Inflammatory signaling has been extensively studied in T cell and macrophage/microglial effects in multiple sclerosis modeling. However, inflammatory cytokine signaling is clearly heterogeneous in its direct effects on OLs (Rodgers et al., 2015), and will require study of the individual pathways to understand their contribution to the brain's response to white matter stroke.

Overall, these data indicate that white matter stroke induces a sequential OPC response within a glial cellular niche adjacent to the infarct that dynamically regulates tissue reorganization and repair and has a role in aged stroke. These findings have relevance to the two major clinical features of white matter stroke: it is strongly linked to aging (even normal aging), and this disease spreads locally to engulf greater adjacent areas of white matter. Aging white matter stroke has reduced nuclear receptor signaling and myelin repair in nonstroke white matter injury, via a decreased activation of the retinoid X receptor pathway (Natrajan et al., 2015). White matter stroke in the aged brain provokes a greater inflammatory response in the injured white matter (Rosenzweig and Carmichael, 2013; Xu et al., 2018), but there has been little evidence for a systemic or generalized increase in brain inflammation in white matter stroke with aging (Aribisala et al., 2014; Chen et al., 2016). The OPC transcriptional data indicate that white matter stroke induces inflammatory signaling locally within the OPCs that border the infarct, developing over time, in a process that may not be detectable using traditional biomarkers of microglial or systemic inflammation. By targeting the unique OPC nuclear receptor and inflammatory responses and modulating astrocyte signaling, the data in the present study suggest distinct avenues that might enhance recovery in this disease.

References

Agresti C, D'Urso D, Levi G (1996) Reversible inhibitory effects of interferon-gamma and tumour necrosis factor-alpha on oligodendroglial lineage cell proliferation and differentiation in vitro. Eur J Neurosci 8:1106–1116.

Aribisala BS, Wiseman S, Morris Z, Valdés-Hernández MC, Royle NA, Maniega SM, Gow AJ, Corley J, Bastin ME, Starr J, Deary IJ, Wardlaw JM (2014) Circulating inflammatory markers are associated with magnetic resonance imaging-visible perivascular spaces but not directly with white matter hyperintensities. Stroke 45:605–607.

Auvergne RM, Sim FJ, Wang S, Chandler-Militello D, Burch J, Al Fanek Y, Davis D, Benraiss A, Walter K, Achanta P, Johnson M, Quinones-Hinojosa A, Natesan S, Ford HL, Goldman SA (2013) Transcriptional differences between normal and glioma-derived glial progenitor cells identify a core set of dysregulated genes. Cell Rep 3:2127–2141.

Baezner H, Blahak C, Poggesi A, Pantoni L, Inzitari D, Chabriat H, Erkinjuntti T, Fazekas F, Ferro JM, Langhorne P, O'Brien J, Scheltens P, Visser MC, Wahlund LO, Waldemar G, Wallin A, Hennerici MG (2008) Association of gait and balance disorders with age-related white matter changes: the LADIS study. Neurology 70:935–942.

Barnett SC, Linington C (2013) Myelination: do astrocytes play a role? Neuroscientist 19:442–450.

Barres BA, Koroshetz WJ, Swartz KJ, Chun LL, Corey DP (1990) Ion channel expression by white matter glia: the O-2A glial progenitor cell. Neuron 4: 507–524.

Cahoy JD, Emery B, Kaushal A, Foo LC, Zamanian JL, Christopherson KS, Xing Y, Lubischer JL, Krieg PA, Krupenko SA, Thompson WJ, Barres BA (2008) A transcriptome database for astrocytes, neurons, and oligodendrocytes: a new resource for understanding brain development and function. J Neurosci 28:264–278.

Chen A, Oakley AE, Monteiro M, Tuomela K, Allan LM, Mukaetova-Ladinska EB, O'Brien JT, Kalaria RN (2016) Multiplex analyte assays to characterize different dementias: brain inflammatory cytokines in post-stroke and other dementias. Neurobiol Aging 38:56–67.

Coban H, Spencer T, Yoo B, Vinters HV, Hinman JD (2017) Molecular disorganization of axons adjacent to human cortical microinfarcts. Front Neurol 8:405.

Dawson MI, Xia Z (2012) The retinoid X receptors and their ligands. Biochim Biophys Acta 1821:21–56.

DeCarli C, Fletcher E, Ramey V, Harvey D, Jagust WJ (2005) Anatomical mapping of white matter hyperintensities (WMH): exploring the relationships between periventricular WMH, deep WMH, and total WMH burden. Stroke 36:50–55.

Dobin A, Davis CA, Schlesinger F, Drenkow J, Zaleski C, Jha S, Batut P, Chaisson M, Gingeras TR (2013) STAR: ultrafast universal RNA-seq aligner. Bioinformatics 29:15–21.

Du X, Tabeta K, Mann N, Crozat K, Mudd S, Beutler B (2005) An essential role for RXR alpha in the development of Th2 responses. Eur J Immunol 35:3414–3423.

Dugas JC, Cuellar TL, Scholze A, Ason B, Ibrahim A, Emery B, Zamanian JL, Foo LC, McManus MT, Barres BA (2010) Dicer1 and miR-219 Are required for normal oligodendrocyte differentiation and myelination. Neuron 65:597–611.

Gallo V, Armstrong RC (2008) Myelin repair strategies: a cellular view. Curr Opin Neurol 21:278–283.

Geller SF, Ge PS, Visel M, Flannery JG (2008) In vitro analysis of promoter activity in Muller cells. Mol Vis 14:691–705.

González-Fernández E, Jeong HK, Fukaya M, Kim H, Khawaja RR, Srivastava IN, Waisman A, Son YJ, Kang SH (2018) PTEN negatively regulates the cell lineage progression from $NG2^+$ glial progenitor to oligodendrocyte via mTOR-independent signaling. Elife 7:e32021.

Gouw AA, van der Flier WM, Fazekas F, van Straaten EC, Pantoni L, Poggesi A, Inzitari D, Erkinjuntti T, Wahlund LO, Waldemar G, Schmidt R, Scheltens P, Barkhof F (2008) Progression of white matter hyperintensities and incidence of new lacunes over a 3-year period: the Leukoaraiosis and Disability Study. Stroke 39:1414–1420.

Hinman JD, Rasband MN, Carmichael ST (2013) Remodeling of the axon initial segment after focal cortical and white matter stroke. Stroke 44:182–189.

Hinman JD, Lee MD, Tung S, Vinters HV, Carmichael ST (2015) Molecular disorganization of axons adjacent to human lacunar infarcts. Brain 138:736–745.

Huang JK, Jarjour AA, Nait Oumesmar B, Kerninon C, Williams A, Krezel W, Kagechika H, Bauer J, Zhao C, Baron-Van Evercooren A, Chambon P, Ffrench-Constant C, Franklin RJ (2011a) Retinoid X receptor gamma signaling accelerates CNS remyelination. Nat Neurosci 14:45–53.

Huang JK, Fancy SP, Zhao C, Rowitch DH, Ffrench-Constant C, Franklin RJ (2011b) Myelin regeneration in multiple sclerosis: targeting endogenous stem cells. Neurotherapeutics 8:650–658.

Iadecola C (2013) The pathobiology of vascular dementia. Neuron 80:844–866.

Jen J, Cohen AH, Yue Q, Stout JT, Vinters HV, Nelson S, Baloh RW. Hereditary endotheliopathy with retinopathy, nephropathy, and stroke (HERNS) (1997) Neurology 49:1322–1330.

Jonas A, Thiem S, Kuhlmann T, Wagener R, Aszodi A, Nowell C, Hagemeier K, Laverick L, Perreau V, Jokubaitis V, Emery B, Kilpatrick T, Butzkueven H, Gresle M (2014) Axonally derived matrilin-2 induces proinflammatory responses that exacerbate autoimmune neuroinflammation. J Clin Invest 124:5042–5056.

Kidd G, Trapp BD (2010) Molecular organization of the oligodendrocyte and myelin. In: The biology of oligodendrocyes (Armati P, Mathey M, eds). Cambridge, UK: Cambridge UP.

Koo BB, Bergethon P, Qiu WQ, Scott T, Hussain M, Rosenberg I, Caplan LR, Bhadelia RA (2012) Clinical prediction of fall risk and white matter abnormalities: a diffusion tensor imaging study. Arch Neurol 69:733–738.

Korpos É, Deák F, Kiss I (2015) Matrilin-2, an extracellular adaptor protein, is needed for the regeneration of muscle, nerve and other tissues. Neural Regen Res 10:866–869.

Langhammer CG, Previtera ML, Sweet ES, Sran SS, Chen M, Firestein BL (2010) Automated Sholl analysis of digitized neuronal morphology at multiple scales: Whole cell Sholl analysis versus Sholl analysis of arbor subregions. Cytometry A 77:1160–1168.

Li S, Overman JJ, Katsman D, Kozlov SV, Donnelly CJ, Twiss JL, Giger RJ, Coppola G, Geschwind DH, Carmichael ST (2010) An age-related axonal sprouting transcriptome in cortical neurons after stroke. Nat Neurosci 13:1496–1504.

Malin D, Sonnenberg-Riethmacher E, Guseva D, Wagener R, Aszódi A, Irintchev A, Riethmacher D (2009) The extracellular-matrix protein matrilin 2 participates in peripheral nerve regeneration. J Cell Sci 122:995–1004.

Montani L, Gerrits B, Gehrig P, Kempf A, Dimou L, Wollscheid B, Schwab ME (2009) Neuronal nogo-A modulates growth cone motility via rho-GTP/LIMK1/cofilin in the unlesioned adult nervous system. J Biol Chem 284:10793–10807.

Nagaraja AK, Middlebrook BS, Rajanahally S, Myers M, Li Q, Matzuk MM, Pangas S (2010) Defective gonadotropin-dependent ovarian folliculogenesis and granulosa cell gene expression in inhibin-deficient mice. Endocrinology 15:4994–5006.

Natrajan MS, de la Fuente AG, Crawford AH, Linehan E, Nuñez V, Johnson KR, Wu T, Fitzgerald DC, Ricote M, Bielekova B, Franklin RJ (2015) Retinoid X receptor activation reverses age-related deficiencies in myelin debris phagocytosis and remyelination. Brain 138:3581–3597.

Nielsen JA, Maric D, Lau P, Barker JL, Hudson LD (2006) Identification of a novel oligodendrocyte cell adhesion protein using gene expression profiling. J Neurosci 26:9881–9991.

Oh LY, Denninger A, Colvin JS, Vyas A, Tole S, Ornitz DM, Bansal R (2003) Fibroblast growth factor receptor 3 signaling regulates the onset of oligodendrocyte terminal differentiation. J Neurosci 23:883–894.

Overman JJ, Clarkson AN, Wanner IB, Overman WT, Eckstein I, Maguire JL, Dinov ID, Toga AW, Carmichael ST (2012) A role for ephrin-A5 in axonal sprouting, recovery, and activity-dependent plasticity after stroke. Proceedings of the National Academy of Science (PNAS) 109:E2230–E2239.

Raff MC, Miller RH, Noble M (1983) A glial progenitor cell that develops in vitro into an astrocyte or an oligodendrocyte depending on culture medium. Nature 303:390–396.

Rajasekharan S, Baker KA, Horn KE, Jarjour AA, Antel JP, Kennedy TE (2009) Netrin 1 and Dcc regulate oligodendrocyte process branching and membrane extension via fyn and RhoA. Development 136:415–426.

Robinson MD, McCarthy DJ, Smyth GK (2010) edgeR: a bioconductor package for differential expression analysis of digital gene expression data. Bioinformatics 26:139–140.

Rodgers JM, Robinson AP, Rosler ES, Lariosa-Willingham K, Persons RE, Dugas JC, Miller SD (2015) IL-17A activates ERK1/2 and enhances differentiation of oligodendrocyte progenitor cells. Glia 63:768–779.

Rosenzweig S, Carmichael ST (2013) Age-dependent exacerbation of white matter stroke outcomes: a role for oxidative damage and inflammatory mediators. Stroke 44:2579–2786.

Schmandke A, Schmandke A, Strittmatter SM (2007) ROCK and rho: biochemistry and neuronal functions of rho-associated protein kinases. Neuroscientist 13:454–469.

Simon C, Götz M, Dimou L (2011) Progenitors in the adult cerebral cortex: cell cycle properties and regulation by physiological stimuli and injury. Glia 59:869–881.

Skory RM, Bernabé BP, Galdones E, Broadbelt LJ, Shea LD, Woodruff TK (2013) Microarray analysis identifies COMP as the most differentially regulated transcript throughout in vitro follicle growth. Mol Rep Dev 80:132–144.

Soumaré A, Elbaz A, Zhu Y, Maillard P, Crivello F, Tavernier B, Dufouil C, Mazoyer B, Tzourio C (2009) White matter lesions volume and motor performances in the elderly. Ann Neurol 65:706–715.

Sozmen EG, Kolekar A, Havton LA, Carmichael ST (2009) A white matter stroke model in the mouse: axonal damage, progenitor responses and MRI correlates. J Neurosci Methods 180:261–272.

Sozmen EG, Rosenzweig S, Llorente IL, DiTullio DJ, Machnicki M, Vinters HV, Havton LA, Giger RJ, Hinman JD, Carmichael ST (2016) Nogo receptor blockade overcomes remyelination failure after white matter stroke and stimulates functional recovery in aged mice. Proc Natl Acad Sci U S A 113:E8453–E8462.

Suresh PS, Rajan T, Tsutsumi R (2011) New targets for old hormones: inhibins clinical role revisited. Endocr J 58:223–235.

Suzumura A, Bhat S, Eccleston PA, Lisak RP, Silberberg DH (1984) The isolation and long-term culture of oligodendrocytes from newborn mouse brain. Brain Res 324:379–383.

Thomas DM, Francescutti-Verbeem DM, Kuhn DM (2006) Gene expression profile of activated microglia under conditions associated with dopamine neuronal damage. FASEB J 20:515–517.

Verghese J, Lipton RB, Hall CB, Kuslansky G, Katz MJ, Buschke H (2002) Abnormality of gait as a predictor of non-Alzheimer's dementia. N Engl J Med 347:1761–1768.

White R, Krämer-Albers EM (2014) Axon-glia interaction and membrane traffic in myelin formation. Front Cell Neurosci 7:284.

Whitman GT, Tang Y, Lin A, Baloh RW, Tang T (2001) A prospective study of cerebral white matter abnormalities in older people with gait dysfunction. Neurology 57:990–994.

Xu M, Wang MM, Gao Y, Keep RF, Shi Y (2018) The effect of age-related risk factors and comorbidities on white matter injury and repair after ischemic stroke. Neurobiol Dis 126:13–22.

Zamanian JL, Xu L, Foo LC, Nouri N, Zhou L, Giffard RG, Barres BA (2012) Genomic analysis of reactive astrogliosis. J Neurosci 32:6391–6410.

Zhang Y, Chen K, Sloan SA, Bennett ML, Scholze AR, O'Keeffe S, Phatnani HP, Guarnieri P, Caneda C, Ruderisch N, Deng S, Liddelow SA, Zhang C, Daneman R, Maniatis T, Barres BA, Wu JQ (2014) An RNAsequencing transcriptome and splicing database of glia, neurons, and vascular cells of the cerebral cortex. J Neurosci 34:11929–11947.

Zhu X, Bergles DE, Nishiyama A (2008) NG2 cells generate both oligodendrocytes and gray matter astrocytes. Development 135:145–157.